SpringerPlus
a SpringerOpen Journal

RESEARCH Open Access

# An approach to predict the risk of glaucoma development by integrating different attribute data

Yuichi Tokuda[1], Tomohito Yagi[1], Kengo Yoshii[1], Yoko Ikeda[2], Masahiro Fuwa[3], Morio Ueno[2], Masakazu Nakano[1], Natsue Omi[1], Masami Tanaka[1], Kazuhiko Mori[2], Masaaki Kageyama[3], Ikumitsu Nagasaki[4], Katsumi Yagi[5], Shigeru Kinoshita[2] and Kei Tashiro[1*]

**Abstract**

Primary open-angle glaucoma (POAG) is one of the major causes of blindness worldwide and considered to be influenced by inherited and environmental factors. Recently, we demonstrated a genome-wide association study for the susceptibility to POAG by comparing patients and controls. In addition, the serum cytokine levels, which are affected by environmental and postnatal factors, could be also obtained in patients as well as in controls, simultaneously. Here, in order to predict the effective diagnosis of POAG, we developed an "integration approach" using different attribute data which were integrated simply with several machine learning methods and random sampling. Two data sets were prepared for this study. The one is the "training data set", which consisted of 42 POAG and 42 controls. The other is the "test data set" consisted of 73 POAG and 52 controls. We first examined for genotype and cytokine data using the training data set with general machine learning methods. After the integration approach was applied, we obtained the stable accuracy, using the support vector machine method with the radial basis function. Although our approach was based on well-known machine learning methods and a simple process, we demonstrated that the integration with two kinds of attributes, genotype and cytokines, was effective and helpful in diagnostic prediction of POAG.

**Keywords:** *Glaucoma*, GWAS, Machine learning, Integration approach

## Introduction

Glaucoma is a progressive eye disease that shows characteristic degeneration of the optic nerve and visual field defects (Kwon et al. 2009). Among the subtypes of glaucoma, primary open-angle glaucoma (POAG) is a major cause of blindness worldwide. The results of many studies have suggested that a genetic contribution is one of the risk factors for the development of glaucoma (Ray & Mookherjee 2009). However, it is still unclear if the genetic risk factors contribute to all of the pathogenesis of glaucoma. To investigate the mechanism(s) of common diseases such as glaucoma, genome-wide association studies (GWAS) have been widely performed (Consortium TWTCC 2007; Balding 2006). GWAS is one of the powerful tools to identify genetic association to common diseases with genotype data for single nucleotide polymorphisms (SNPs). Previously, we performed a GWAS to identify the common POAG-associated genetic factors (Nakano et al. 2009) and found a number of SNPs significantly associated with POAG. GWAS for POAG has also been performed by several other research groups (Meguro et al. 2010; Thorleifsson et al. 2010; Burdon et al. 2011), and we also recently published additional GWAS research results on POAG (Nakano et al. 2012). However, compared with the genetic risk for another type of glaucoma, Exfoliation Glaucoma (EG), which was carried out by deCODE using only two SNPs (http://www.decodehealth.com/glaucoma), genetic contribution for POAG seems to be a complex. In EG, SNPs were highly significant on a single gene, LOXL1, by GWAS (Thorleifsson et al. 2007; Williams et al. 2010; Mabuchi et al. 2008; Fan

* Correspondence: tashiro@koto.kpu-m.ac.jp
[1]Department of Genomic Medical Sciences, Kyoto Prefectural University of Medicine, Kajiicho 465, Kawaramachi-Hirokoji, Kamigyo-ku, Kyoto 602-8566, Japan
Full list of author information is available at the end of the article

et al. 2008), while in POAG, several genes are involved as genetic risk factors. In addition, besides the genetic factor, POAG is considered to have other risk factors (Kwon et al. 2009) as well. Thus, precise disease mechanism(s) of POAG remains elusive.

For the purposes of diagnostic prediction or finding out the pathogenesis of diseases, genotype data have been applied in several machine-learning algorithms (Relton et al. 2004; Listgarten et al. 2004; Ritchie et al. 2001; Nelson et al. 2001; Hoh et al. 2001; Wang et al. 2012). Genetic data and the other risk factors (e.g., smoking, body mass index) were combined for these prediction models (Seddon et al. 2009). In such studies, careful extraction of attributes for prediction from large volumes of data and appropriate data selection from several attributes are essential. As the development of common diseases like POAG is influenced by many factors, the contribution of each attribute weighs variously among the patients. Thus, for the diagnostic prediction of POAG, clarification of each attribute obtained for analysis needs to be carefully assessed. In this regard, it is important to develop a new strategy of integrating the data with various attributes for establishing useful diagnostic prediction.

In order to evaluate the risk factor of POAG, we integrated cytokine data together with genetic data as a new strategy. We focused on the serum cytokines because the relation between glaucomatous neurodegeneration and immune response was previously suggested (Tezel 2011), and several cytokines were reported to be linked with glaucoma (Huang et al. 2010; Yang et al. 2001). Cytokines, which include both chemokines and lymphokines, are small soluble proteins that play a pivotal role in immune system. The concentration of serum cytokines may reflect the physiological condition of the hosts affected by environmental and postnatal factors as one of the important indices useful for the diagnostic prediction of certain diseases. Obviously, cytokine data as an attribute weigh differently from those of the genotype data. In addition, the equipments that many cytokines can measure simultaneously under the same condition could have been developed and applied to diagnostic analysis (Ray et al. 2007; Lambeck et al. 2007). Therefore, we especially tried to measure and handle many cytokines simultaneously.

Here, for predicting the risk of POAG development, we attempted to establish a new integration approach with a good potential as a useful and simple tool. This procedure performs the integration of data with various kinds of attributes by using several machine learning methods with random sampling. In particular, because both genotyping and cytokines attributes were obtained from blood sample, our approach is considered to be useful for assessment of the risk of POAG and predicting the onset possibility before consulting ophthalmologists. This strategy may give us with new prototype for a clinical approach in understanding the underlying mechanism(s) of various diseases, not limited to POAG.

## Methods

### Sample Information

To obtain the peripheral blood samples, 115 POAG patients and 94 healthy control volunteers were recruited at the University Hospital of Kyoto Prefectural University of Medicine (Kyoto, Japan). This study was approved by the institutional review board of Kyoto Prefectural University of Medicine and conducted in accordance with the principles set forth in the Helsinki Declaration. All participants were interviewed about their familial history of glaucoma and other diseases and diagnosed either POAG or control by three ophthalmologists (YI, MU, and KM). The 115 POAG patients had peak intraocular pressure ≥ 22 mmHg without treatment. Peripheral blood samples were collected simultaneously from each participant for obtaining genomic DNA for genotyping and serum for cytokine measurement. DNA and sera were stored at −80°C until examined.

These samples were divided into two groups, since the cytokine data was obtained with two conditions. The first was defined as the "training data set" and the other as the "test data set" (Table 1). The former consisted of 42 POAG and 42 healthy control samples and was utilized in the training process of the machine learning. The latter consisted of 73 POAG and 52 healthy control samples, which were applied for the diagnostic prediction of POAG.

### Genotype data

All genotype data were obtained by GeneChip® Human Mapping 500K Array platform (Affymetrix) according to the manufacturer's instructions. Although this array system carries the probes for more than five hundred thousand SNPs, we needed a number of SNPs significantly associated with POAG for the tests. Our previous study (Nakano et al. 2009) suggested that 40 SNPs were significantly POAG-associated which had both Mantel-Haenszel p-value of less than 0.01 and a p-value of Cochran's Q test (Ioannidis et al. 2007) equal to or more than 0.05 in the two stage GWAS. Because the pairs of SNPs showing high linkage disequilibrium (LD) could cause a multicollinearity problem, the Haploview program (Barrett et al. 2005) was applied to calculate LD. As a result, 11 of the 40 SNPs were excluded because of their high LD and remaining 29 SNPs were employed in this study (Table 2). All of the genotype data except for the missing by genotyping failure, which were

**Table 1 Clinical characteristic of samples**

| | Training data set | | Test data set | |
|---|---|---|---|---|
| | POAG | Control | POAG | Control |
| Number of sample | 42 | 42 | 73 | 52 |
| Famale / male ratio | 1.00 | 0.83 | 0.62 | 1.74 |
| Age at blood sampling | 56.4±5.5 | 55.3±3.4 | 70.9±10.7 | 61.8 ± 11.3 |
| Storage period of blood (days) | 880.1±112.0 | 865.7±106.0 | 1044.0±114.4 | 892.2 ± 129.9 |

represented by a pair of letters (e.g., AA, AT and TT), were converted into discrete numerical values according to the number of allele with higher frequency in the POAG (i.e., risk allele) as followed: risk allele homozygote, 2; risk allele heterozygote, 1; and other allele homozygote, 0. Then, all the genotype data were normalized using the equations in EIGENSTRAT (Price et al. 2006), so that the missing data were set to 0.0. According to the allele frequency and the average of numeric genotypes calculated from the training data set, this normalization was carried out and the normalized data represented discrete values.

**Table 2 Summary of 29 SNPs used in this study**

| dbSNP ID | Chr. | SNP type | Nearest gene | Genotype frequency |
|---|---|---|---|---|
| rs547984 | 1 | intergenic | ZP4 | AA(0.263) AC(0.488) CC(0.249) |
| rs1892116 | 1 | intronic | AHCTF1 | AA(0.507) AG(0.445) GG(0.048) |
| rs4666488 | 2 | intergenic | OSR1 | AA(0.100) AG(0.397) GG(0.503) |
| rs2268794 | 2 | intronic | SRD5A2 | AA(0.005) AT(0.319) TT(0.676) |
| rs7574012 | 2 | intergenic | QPCT | AA(0.373) AG(0.459) GG(0.168) |
| rs1990702 | 2 | intergenic | LRP2 | GG(0.120) GA(0.433) AA(0.447) |
| rs10930437 | 2 | intergenic | SP5 | AA(0.429) AG(0.454) GG(0.117) |
| rs779701 | 3 | intronic | GRM7 | AA(0.490) AG(0.413) GG(0.097) |
| rs6550783 | 3 | intergenic | UBE2E1 | AA(0.412) AG(0.442) GG(0.146) |
| rs6550308 | 3 | intergenic | ARPP21 | GG(0.215) GA(0.488) AA(0.297) |
| rs3922704 | 3 | intronic | PLCXD2 | CC(0.034) CG(0.254) GG(0.712) |
| rs17279573 | 4 | intergenic | KIAA0922 | GG(0.120) GA(0.483) AA(0.397) |
| rs818725 | 5 | intronic | ADAMTS12 | CC(0.019) CG(0.226) GG(0.755) |
| rs11750584 | 5 | intergenic | HEATR7B2 | CC(0.029) CG(0.292) GG(0.679) |
| rs9640055 | 7 | intronic | GLCCI1 | GG(0.038) GA(0.344) AA(0.618) |
| rs2966712 | 7 | intergenic | LOC285965 | AA(0.005) AG(0.211) GG(0.784) |
| rs411102 | 9 | intergenic | KRT8P11 | GG(0.749) GA(0.242) AA(0.009) |
| rs7850541 | 9 | intergenic | GBGT1 | GG(0.514) GA(0.361) AA(0.125) |
| rs7081455 | 10 | intergenic | PLXDC2 | AA(0.644) AC(0.293) CC(0.063) |
| rs493622 | 11 | intergenic | CHORDC1 | AA(0.565) AC(0.383) CC(0.052) |
| rs610160 | 11 | intronic | GRIA4 | AA(0.693) AG(0.262) GG(0.045) |
| rs7961953 | 12 | intronic | TMTC2 | GG(0.522) GA(0.397) AA(0.081) |
| rs10492680 | 13 | intergenic | FLJ42392 | GG(0.005) GA(0.187) AA(0.808) |
| rs1571379 | 14 | intergenic | SEL1L | AA(0.440) AG(0.454) GG(0.106) |
| rs9788983 | 17 | intronic | RPH3AL | AA(0.770) AG(0.215) GG(0.015) |
| rs16940484 | 18 | intronic | TTC39C | GG(0.469) GA(0.450) AA(0.081) |
| rs2864107 | 19 | intergenic | ZNF175 | GG(0.684) GA(0.301) AA(0.015) |
| rs6115865 | 20 | intergenic | C20orf194 | AA(0.125) AG(0.428) GG(0.447) |
| rs5765558 | 22 | intergenic | ATXN10 | AA(0.287) AG(0.478) GG(0.235) |

The dbSNP ID represents with build 130. Chr. denotes the number of chromosome. The Nearest genes are positioned nearest by each SNP and referred to NCBI Build 36. Genotype frequencies are calculated by total samples used in this study, which are 115 POAG patients and 94 healthy control volunteers.

### Cytokine data

Serum cytokines were measured by the bead flow-cytometry analysis by the Becton Dickinson (BD, San Diego, CA) Cytometric Bead Array (CBA™) Flex Set System according to the manufacturer's protocol. The data was examined by a BD FACSArray™ (BD) flow cytometer with FCAP Array™ software and the BD FACSArray™ Bioanalyzer (BD).

In this study, we first assayed 29 cytokines in the sera from "the training data set", and each cytokine concentration was calculated from each raw data by the Four Parameter Logistic Model (FPLM), which was recommended by the manufacturer (http://www.bdbiosciences.com/documents/Analysis_of_data_from_CBA_using_FCAPArray.pdf). Before we performed the statistical analysis, the quality of the cytokine data was evaluated. Of 29 cytokines, 21 cytokines were excluded; 7 were for measurement failures (over 5% of the 84 samples) and 14 for concentration of zero (over 5% of the 84 samples). The remaining 8 cytokines were tested by the Student's *t*-test between the POAG and control samples, of which 5 cytokines were excluded with a p-value over 5%. Eventually, only 3 cytokines, i.e., Fas Ligand, Eotaxin, and MIG, were picked up to be significantly associated with POAG from the training data set samples (Table 3).

Subsequently, these 3 cytokines were determined with the same assay procedure on 126 samples (73 POAG and 53 controls) from the "test data set" samples. Data were obtained from 125 samples, excluding one control sample of failed assay (Table 3). For statistical analysis, the cytokine concentration data were standardized in order to minimize the biases among the assay conditions as followed. Let $c_{ij}$ be the cytokine concentration measured for cytokine $i$ and sample $j$, where $i = 1$ to 3 and $j = 1$ to $M$ ($M$ is 84 in the training data set; 125 in the test data set). Let $m_i$ and $s_i$ be the mean and standard deviation of cytokine $i$, respectively. At each data set, $m_i$ and $s_i$ were calculated only for the control samples because it was considered that the cytokine concentration of healthy control samples might act fairly consistently under each experimental condition. The standardized value $n_{ij}$ was calculated using the following equation: $n_{ij} = (c_{ij} - m_i)/s_i$. Notably, the cytokine concentration data was obtained as continuous values when they were calculated by FPLM.

Finally, results of a total of 32 attributes, which consisted of 29 SNPs (Table 2) and 3 cytokines (Table 3), were applied for "integration approach" in this study.

### Base classifiers

In this study, well-known machine learning methods, i.e., Linear Discriminant Analysis (LDA), Support Vector Machine (SVM), Naive Bayes Classifier (NBC), and Decision Tree (DT) were applied. We defined these methods as "base classifiers".

LDA is a method used in statistics and machine learning to find a discriminant function by which two or more groups can be separated. LDA seeks a linear function of the variables (e.g., genotype and cytokine) in the training data set that maximizes the distance among means in each group as it minimizes the within-group variance. Hence, a discriminant function can be computed explicitly and used as a linear classifier.

SVM is a supervised machine learning method based on the idea of classifying two groups by a hyperplane with a large margin. SVM maps the data in the training data set into a possibly higher dimension of space by using a kernel function. In the space, SVM learns the classifier by seeking a hyperplane that may separate the two groups by a certain distance. If the training data set is not separated linearly, SVM optimizes the separation between the two groups. The kernel function in SVM is decided according to the attribute of the data. In this study, we used SVM for learning with three kernel functions: linear, polynomial, and radial basis function (RBF).

NBC is a simple and efficient probabilistic classifier based on Bayes' theorem. Assuming there is independence between each set of attribute data (e.g., genotype or cytokine); NBC calculates the probabilities used for the prediction from the training data set. As each sample in the test data set is given to the NBC, it predicts to which

**Table 3 Summary of the three cytokines used in the integration approach**

| Cytokine | | Training data set | | Test data set | |
|---|---|---|---|---|---|
| | | Concentration | P-value* | Concentration | P-value* |
| Fas Ligand | POAG | 63.5 (52.2-87.3) | 0.002 | 37.5 (31.8-46.6) | 0.877 |
| | Control | 53.3 (34.9-63.4) | | 36.2 (28.0-45.4) | |
| Eotaxin | POAG | 309.1 (273.6-342.9) | 0.038 | 70.6 (54.9-90.8) | 0.013 |
| | Control | 268.5 (236.7-311.6) | | 63.5 (54.4-73.9) | |
| MIG | POAG | 410.9 (306.8-524.9) | 0.021 | 318.1 (182.9-511.7) | 0.109 |
| | Control | 340.4 (198.9-470.1) | | 148.4 (117.7-241.9) | |

"Concentration" represents the median concentration and interquartile range. * P-value of the comparison between POAG and control calculated by Student's *t*-test.

group (e.g., POAG or control) the sample belongs by the highest conditional probability.

DT is a tree-like data structure used for learning a method to classify data hierarchically by sequential decision process. Basically, DT is a binary tree and each node splits the data by each feature (i.e., large/small, male/female). In this study, DT was performed by CART (Classification and Regression Trees), and used to classify SNPs (each data consisted four discrete; three genotypes and missing data) and cytokines (each data was continuous).

All the data analysis and drawing figures were performed with R software (version 2.14.0) (R Development Core Team 2011); the LDA was implemented by the MASS (version 7.3-16) R package; the SVM and NBC functions were implemented by the e1071 (version 1.6) R package (Dimitriadou et al. 2011); and the DT functions were implemented by the mvpart (version 1.4-0) R package. In addition, each classifier was performed with default parameter settings.

Accuracy, sensitivity and specificity of the data (genotype and cytokine) for the POAG prediction were calculated by these analytical procedures.

### Integration approach

In this study, the data consists of two kinds of attributes in that the genotype data are discrete and the cytokine data are continuous. In most cases, it is easy and no problem to apply these data for each method simply and simultaneously. However, one must be careful to integrate them while considering each attribute, especially to note how each attribute contributes. The prediction may be made possible from analytical results for each type of attribute data instead of applying the data directly, because of the difference in the attributes. In addition, if the analytical results show differences between each attribute, the prediction for each sample has interesting information how each attribute contributes. For these reasons, we performed the integration approach so that after the genotype and cytokine data are separately applied in the processes, their results are integrated after the last process. To enable an effective analysis by integrating these two kinds of data, this approach is based on the idea of ensemble learning (e.g., Bootstrap aggregating (Bagging) (Breiman 1996)). Bagging is one of the powerful prediction tools for improving other basic classifier. For example, bagging is used for the purpose of improving the diagnosis of Valvular Heart Disease by SVM (Sengur 2012), or assessing the interactions of SNPs (Schwender et al. 2011).

For the training data set $L$ consisted of cases $(l_1^P,\ldots,l_p^P)$ and controls $(l_1^c,\ldots,l_q^c)$ and the test data set $T = \{t_1,\ldots,t_r\}$, the integration approach consists of the following steps:

1) Obtain $Sg$, which is the subset of the training data set, by random sampling without replacement from $L$ so that the same number of samplings is taken from the cases as from the controls.
2) Apply the base classifiers to the genotype data of $Sg$ to obtain a predictor $Pg$ as a training result.
3) Repeat above steps (1) and (2) $K$ times; this process produces genotype data predictors $\{Pg_1,\ldots,Pg_K\}$ from $\{Sg_1,\ldots,Sg_K\}$.
4) In addition, repeat the same process as in (1) and (2) above $N$ times for cytokine data; cytokine data predictors $\{Pc_1,\ldots,Pc_N\}$ are produced from the subset of the training data set $\{Sc_1,\ldots,Sc_N\}$.
5) For each $t_j$ in the test data $T$, the predictor gives a result which predicts whether $t_j$ belongs to the cases (positive) or the controls (negative). Thus for each $t_j$ in the test data $T$, the genotype data predictors $\{Pg_1,\ldots,Pg_K\}$ produce $K$ prediction results $\{Rg_1,\ldots,Rg_K\}$ and the cytokine data predictors $\{Pc_1,\ldots,Pc_N\}$ produce $N$ prediction results $\{Rc_1,\ldots,Rc_N\}$.
6) For each $t_j$ in the test data $T$, the majority vote of the $N + K$ prediction results is the final prediction for $t_j$.

This procedure adopted the same number of samplings, for example, 20 POAG and 20 healthy controls were sampled from 42 POAG and 42 healthy controls in the training data set, respectively. This reason is that the contribution of the characteristics of POAG and control should be as close to equal possible. Besides, it is preferable for the genotype and cytokine data to be evaluated as equally as possible (e.g., $K = N$.) However, it may be impossible to predict one group by dividing it in half if the total number of sampling repeats is an even number. In this study, since the size of the genotype data set was greater than that of the cytokines, $K$ is taken as $N + 1$ to avoid the situation of a tie vote. In addition, note that use of the base classifier should be limited to one kind of classifier from the beginning of this procedure to the end.

## Results

### Single classifier analysis

Single classifier analysis was performed for each base classifier on 29 SNPs and 3 cytokines each and both integrated (Table 4). All of these tests were first done by the training data set and evaluated to predict the test data set. Except for DT, the accuracy of genotype data prediction was higher than that of cytokines for each base classifier. The integrated accuracy was better than each base classifier, when tested with use of the polynomial SVM, RBF SVM, and NBC. However, the integrated sensitivity (0.521) was lower than the genotype (0.589) or cytokine (0.658) prediction alone, when tested by polynomial SVM, in spite of increasing the integrated specificity (0.846) from the genotype (0.731) or cytokine (0.308) prediction alone. By contrast, RBF SVM test

**Table 4 Summary of the three cytokines used in the integration approach**

| Base classifier | | | Single analysis | | | Analysis with sampling* | | |
|---|---|---|---|---|---|---|---|---|
| | | | Accuracy | Sensitivity | Specificity | Accuracy | Sensitivity | Specificity |
| LDA | | Genotype | 0.688 | 0.712 | 0.654 | 0.671 ± 0.011 | 0.693 ± 0.015 | 0.639 ± 0.014 |
| | | Cytokine | 0.592 | 0.466 | 0.769 | 0.584 ± 0.010 | 0.457 ± 0.012 | 0.763 ± 0.010 |
| | | Integrated | 0.632 | 0.616 | 0.654 | 0.655 ± 0.022 | 0.611 ± 0.034 | 0.717 ± 0.015 |
| SVM | linear | Genotype | 0.664 | 0.699 | 0.615 | 0.683 ± 0.013 | 0.754 ± 0.023 | 0.584 ± 0.016 |
| | | Cytokine | 0.568 | 0.452 | 0.731 | 0.577 ± 0.008 | 0.458 ± 0.012 | 0.745 ± 0.013 |
| | | Integrated | 0.659 | 0.648 | 0.673 | 0.668 ± 0.014 | 0.640 ± 0.024 | 0.706 ± 0.012 |
| | polynomial | Genotype | 0.648 | 0.589 | 0.731 | 0.633 ± 0.010 | 0.539 ± 0.026 | 0.764 ± 0.018 |
| | | Cytokine | 0.512 | 0.658 | 0.308 | 0.457 ± 0.012 | 0.275 ± 0.077 | 0.713 ± 0.086 |
| | | Integrated | 0.656 | 0.521 | 0.846 | 0.624 ± 0.010 | 0.480 ± 0.065 | 0.827 ± 0.078 |
| | RBF | Genotype | 0.688 | 0.712 | 0.654 | 0.676 ± 0.010 | 0.685 ± 0.016 | 0.664 ± 0.013 |
| | | Cytokine | 0.648 | 0.712 | 0.558 | 0.662 ± 0.006 | 0.701 ± 0.011 | 0.607 ± 0.020 |
| | | Integrated | 0.744 | 0.767 | 0.712 | 0.740 ± 0.013 | 0.805 ± 0.020 | 0.650 ± 0.014 |
| NBC | | Genotype | 0.640 | 0.671 | 0.596 | 0.630 ± 0.006 | 0.651 ± 0.013 | 0.601 ± 0.014 |
| | | Cytokine | 0.624 | 0.479 | 0.827 | 0.621 ± 0.006 | 0.489 ± 0.013 | 0.807 ± 0.019 |
| | | Integrated | 0.744 | 0.767 | 0.712 | 0.698 ± 0.013 | 0.644 ± 0.027 | 0.775 ± 0.051 |
| DT | | Genotype | 0.536 | 0.342 | 0.808 | 0.562 ± 0.025 | 0.411 ± 0.070 | 0.774 ± 0.043 |
| | | Cytokine | 0.624 | 0.904 | 0.231 | 0.605 ± 0.018 | 0.874 ± 0.099 | 0.226 ± 0.126 |
| | | Integrated | 0.600 | 0.959 | 0.096 | 0.617 ± 0.013 | 0.668 ± 0.032 | 0.545 ± 0.040 |

*These values are represented as the mean and SD of each statistics. The mean of each statistics included extremely good or bad result, especially small sampling size and few sampling repeat time.

increased all of the accuracy (0.744), sensitivity (0.767) and specificity (0.712) on the integrated data from either genotype or cytokine prediction. These results suggested that both genotype and cytokine attributes contributed, especially when integrated, to improve the diagnostic prediction based on the base classifier.

### Integration approach analysis

The results of single use with base classifier demonstrated fluctuations on each or both applying attribute (Table 4; Single analysis). Therefore, the further integrated approach was performed using each base classifier by changing the size and time of parameters (Table 4; Analysis with sampling). One of the changed parameters was the size of the subset sampling from the training data set (defined as "sampling size"), and the other was the sampling repeat times (defined as "sampling time"). The sampling size was increased from 40 (consisted of 20 POAG and 20 healthy controls) to 80 (consisted of 40 POAG and 40 healthy controls) with an equal number of samples from POAG and controls. (i.e., 21 steps were tested) On the other hand, the sampling time for each genotype and cytokine was also increased from 25 to 1,500 by 60 steps. (i.e., 25, 50, 75, ···, 1,450, 1,475 and 1,500 repeat times were tested) Moreover, because the sampling time for the genotype data was increased by one, the total sampling repeat times increased from 51 to 3,001. As a result, the integration approach was performed on 1,260 tests (21 steps of sampling sizes × 60 steps of sampling times) per each base classifier.

These results are summarized in "Analysis with sampling" in Table 4. The LDA, Linear SVM, and DT methods improved the mean of integrated accuracy from single analysis (from 0.632 to 0.655, from 0.659 to 0.668, and from 0.600 to 0.617, respectively), although those values included fluctuations due to parameter settings. The mean of the integrated accuracy (0.740 ± 0.013; mean ± SD) assessed by the RBF SVM method was the best results in analysis with sampling, however, it was slightly lower than that in single analysis in association with the higher integrated sensitivity (0.805 ± 0.020) than that in single analysis (0.767). Moreover, the specificities of genotype (0.664 ± 0.013) and cytokine (0.607 ± 0.020) by SVM RBF method in analysis with sampling were better than those in single analysis (0.654 and 0.558, respectively). In addition, some accuracy in the 1,260 tests was achieved over the single analysis.

In order to understand how the test results improved by changing the sampling size and time of parameters and each attribute contributed to the prediction, the integration results were demonstrated graphically (Figure 1). The schematic presentations of the genotype and cytokine data were plotted on horizontal and vertical axes, respectively, as

shown in Figure 1a. One example of the unstable results was shown in Figure 1b. Because those parameters were comparatively smaller, the positive ratios of each attribute were generally unsatisfactory with several samples being plotted in the vicinity of the diagonal threshold. By contrast, when the sampling size was 70 (consisted of 35 POAG and 35 healthy controls) and sampling times was 2,001 (1,001 times at genotype data and 1,000 times at cytokine data), most of the samples were plotted in the vicinity of the axes (Figure 1c). Using these parameters, the accuracy was improved for 0.768. This result was also obtained by many other conditions when the sampling size and time were comparatively larger; therefore it was considered as the best stable results of the integration approach. Thus, the predictions were improved by changing the size and time of parameters in either the genotype or cytokine test.

In these test plot presentations, we focused on the contribution of the genotype and cytokine data to the

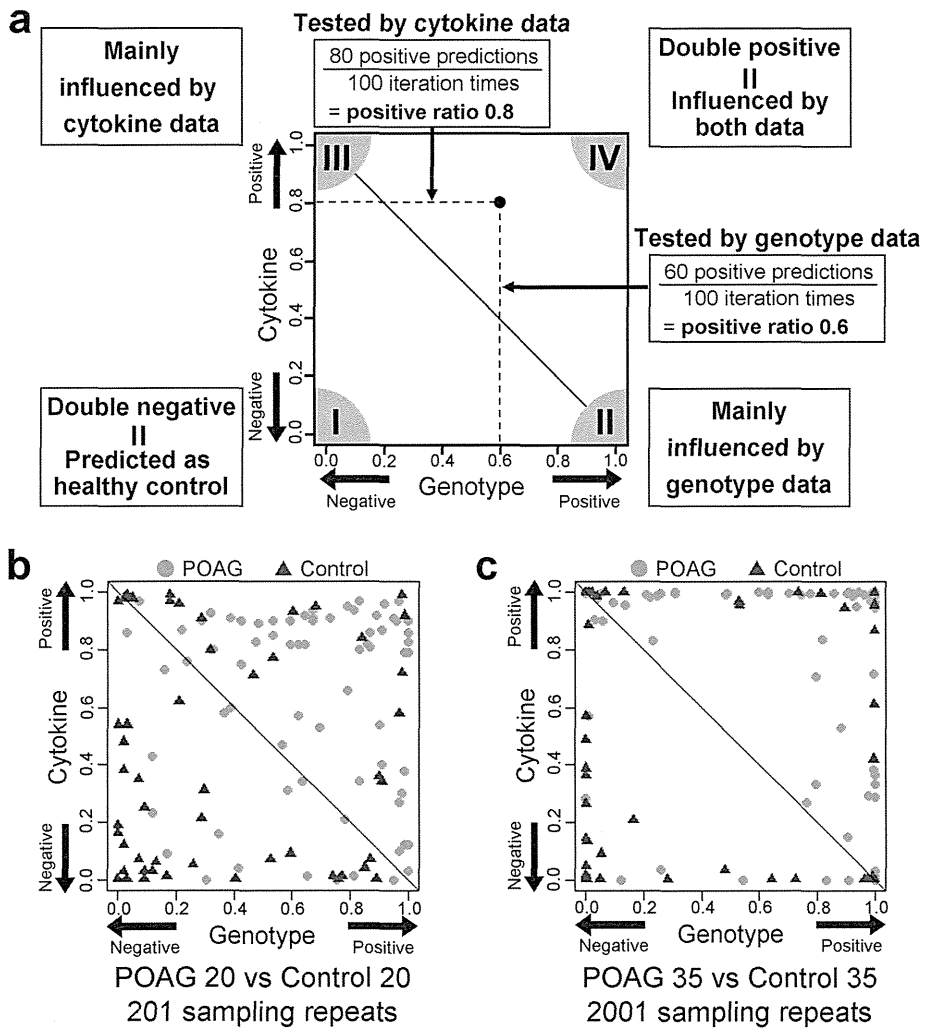


**Figure 1 Scatter plot showing the ratio of POAG prediction for each sample.** Figure 1 (**a**) The example figure for the scatter plot. The horizontal axis represents the ratio of positive prediction using genotype data. The positive prediction indicated the sample with POAG feature, and the negative prediction indicated the sample with control feature. The ratio was obtained by dividing the number of positive predictions by the total test number. Thus, "1" and "0" indicate 100% prediction as positive and negative, respectively. The vertical axis similarly represents the ratio using the cytokine data. Dots and triangles represent POAG and control samples, respectively. The figure can be read as, if one POAG sample was predicted as positive 60 times using the genotype data and 80 times using the cytokine data each with 100 sampling repeat times, the sample is plotted at (0.6, 0.8) by dot. If the approach has a good performance (means; highly negative or positive prediction) for samples with interaction between those two attributes, more samples will be plotted in the corner I or corner IV. If either the genotype or cytokine data is at risk for POAG, such samples will be plotted in the corner II or corner III, respectively. The diagonal line shows the threshold of the prediction by the integration approach. If a sample is plotted above or below the threshold, the final prediction result is positive or negative, respectively. Figure 1 (**b**) shows one of the examples as the comparatively smaller and unstable, which is the result with 40 sampling size and 201sampling times by RBF SVM method. Figure 1 (**c**), one of the examples as the best stable result, which is the result with 70 sampling size and 2,001sampling times by RBF SVM method.

stable results among the POAG samples, 23 (31.5%) showed more than 90% accuracy for both positive ratios (i.e., plotted in the corner IV in Figure 1c). On the other hand, 14 (26.9%) of the control samples showed more than 90% accuracy (i.e., plotted in the corner I in Figure 1c).

## Discussion

Bootstrap methods, such as Bagging (Breiman 1996), are generally applied in approaches using random sampling techniques. In a typical procedure, bootstrap can provide us with an estimated distribution for statistical analysis by random sampling with replacement from all samples in the data set. In this study, the method of random sampling was independent for each group, and an equal number of samples were adopted in order to avoid bias by the difference in sample numbers among each group. Additionally, our approach adopted random sampling without replacement due to the potential for multicollinearity. Because genotype data show discrete values consisted of three genotypes and one missing data, the combinations of values were easy to be limited as much as causing multicollinearity. Especially, this phenomenon was apparent when LDA method was applied with the small sampling size. For this reason, the changing parameters of the sampling size were started with 40 samples by random sampling without replacement. Besides, the accuracy did not improve without any relation to the iteration times even when the sampling size was increased enough as showed in Figure 1c. This tendency was considered to be caused by highly correlated samples. To solve this problem, it might be better to adopt the data for random sampling with replacement than without replacement according to the size of the training data set.

Using genotype data, the diagnostic prediction of POAG by RBF SVM method generally performed well also in our study (Ban et al. 2010; Rojas et al. 2009). The applied 29 SNPs were selected by the statistical result of GWAS from enormous genotype data. Employment of the SNPs selected by some large size of population was useful for this type of diagnostic prediction study without complex procedures. Thus, simple strategy might be suitable for the post GWAS analysis. The bagging is generally considered to reduce variance of classifier such as DT method; therefore, the classifier with less variant such as SVM method was considered to be improved a little by bagging. However the result of our study was effective even when SVM, DT methods with bagging was not improved.

Using cytokine data, the diagnostic prediction of POAG by RBF SVM method also performed well, regardless of some fluctuation between two data sets. Thus, RBF SVM method was thought to be successfully suitable for each attribute data, genotype as well as cytokine, in our study. In other words, the base classifier is necessary to select suitably according to each attribute. However, the effectiveness of cytokine data analysis using SVM has been reported for selecting the significant cytokines to elucidate the pathway of inflammatory response (McKinney et al. 2006).

In this study, we found 3 cytokines that are associated with POAG in 29 cytokines. In our approach, some samples was certainly predicted by only cytokine attributes as shown in Figure 1b or c. These results demonstrated that POAG patients with low genetic risk were predicted by cytokine attributes effectively.

In terms of the integration approach, one of our goals is to predict the diagnosis and/or prognosis by the patterning of different types of experimental data. In the process, an interaction between genotype and cytokine might indicate a risk of disease development, because approximately 30% of the samples in the test data set were performed with a high prediction from both types of data. Our approach also elicited a good classification of same sample when one of the two data sets was used individually before integrating them. The classification was made successful by using one data set because either genotype or cytokine behaved as a risk of disease development in these samples. For such reasons, our approach is considered to be one of the good tools to analyze the mixed data, irrespective of their interaction.

In conclusion, we demonstrated that our integration approach improved the diagnostic prediction of POAG with use of two attributes, SNPs as genotype and serum cytokines. Although two attribute data are applied independently, this approach is not affected by the differences of attribute, because the base classifier was first set according to each type of attribute data. It was confirmed that when the setting of the base classifier for one data set is successfully optimized, the integration approach might be applied using additional data with other attributes. In view of the versatility and simplicity, our approach was thought to be effective and useful for various clinical applications in future.

### Competing interests

The authors declare that they have no conflict of interest.

### Authors' contributions

KM, MK, IN, SK, and KT designed the research. YI, MU, KM, SK and KT recruited POAG patients and healthy volunteers. YI, MU and KM performed their clinical diagnosis, and collected and managed blood samples with NO. NO and MT processed blood samples and prepared DNA samples. MN, NO and MT analyzed and processed the genotyping data. TY, MF and MT measured and analyzed the cytokine data. YT, TY and KYoshii preprocessed and evaluated the genotype and cytokine data. YT and KYoshii developed and improved the integration approach and base classifiers used in it. IN and KYagi helped evaluate the integration approach. YT and TY drafted the manuscript. All the authors read and approved the final manuscript.

### Acknowledgements

We appreciate all the patients and volunteers enrolled in our study. We also thank Ms. Sayaka Ohashi, Naoko Saito, Hiroko Adachi, Yumi Yamashita, and Yuko Konoshima for processing blood samples and performing genotyping;

Mrs. Hiromi Yamada, Ms. Aiko Hashimoto, Ms. Keiko Nirasawa, and Mrs. Akemi Tanaka for assisting with the clinical information analysis; Mr. Ryuichi Sato and Ms. Fumiko Sato (SASA Plus Co., Ltd., Fukuoka, Japan) for the management of genotyping data; and Ms. Tomoko Ichikawa for excellent secretarial assistance. This work was supported by grants from Collaborative Development of Innovative Seeds of Japan Science and Technology Agency (JST) to MK and KT, and Researches on Sensory and Communicative Disorders from the Ministry of Health, Labour and Welfare in Japan to KM, IN, SK, and KT.

**Author details**
[1]Department of Genomic Medical Sciences, Kyoto Prefectural University of Medicine, Kajiicho 465, Kawaramachi-Hirokoji, Kamigyo-ku, Kyoto 602-8566, Japan. [2]Department of Ophthalmology, Kyoto Prefectural University of Medicine, Kajiicho 465, Kawaramachi-Hirokoji, Kamigyo-ku, Kyoto 602-8566, Japan. [3]Research and Development Center, Santen Pharmaceutical Co. Ltd, 8916-16 Takayama-cho, Ikoma, Nara 630-0101, Japan. [4]Department of Mathematics, Kyoto Prefectural University of Medicine, Kajiicho 465, Kawaramachi-Hirokoji, Kamigyo-ku, Kyoto 602-8566, Japan. [5]Louis Pasteur Center for Medical Research, 103-5, Tanakamonzen-cho, Sakyo-ku, Kyoto City, Kyoto 606-8225, Japan.

Received: 29 June 2012 Accepted: 15 October 2012
Published: 24 October 2012

**References**

Balding DJ (2006) A tutorial on statistical methods for population association studies. Nat Rev Genet 7(10):781–791. doi:nrg1916 [pii] 10.1038/nrg1916

Ban HJ, Heo JY, Oh KS, Park KJ (2010) Identification of type 2 diabetes-associated combination of SNPs using support vector machine. BMC Genet 11:26. doi:1471-2156-11-26 [pii] 10.1186/1471-2156-11-26

Barrett JC, Fry B, Maller J, Daly MJ (2005) Haploview: analysis and visualization of LD and haplotype maps. Bioinformatics 21(2):263–265. doi:10.1093/bioinformatics/bth457 bth457 [pii]

Breiman L (1996) Bagging Predictors. Mach Learn 24(2):123–140. doi:10.1023/a:1018054314350

Burdon KP, Macgregor S, Hewitt AW, Sharma S, Chidlow G, Mills RA, Danoy P, Casson R, Viswanathan AC, Liu JZ, Landers J, Henders AK, Wood J, Souzeau E, Crawford A, Leo P, Wang JJ, Rochtchina E, Nyholt DR, Martin NG, Montgomery GW, Mitchell P, Brown MA, Mackey DA, Craig JE (2011) Genome-wide association study identifies susceptibility loci for open angle glaucoma at TMCO1 and CDKN2B-AS1. Nat Genet 43(6):574–578. doi:ng.824 [pii] 10.1038/ng.824

Consortium TWTCC (2007) Genome-wide association study of 14,000 cases of seven common diseases and 3,000 shared controls. Nature 447(7145):661–678. doi:nature05911 [pii] 10.1038/nature05911

Dimitriadou E, Hornik K, Leisch F, Meyer D, Weingessel A (2011) e1071: Misc Functions of the Department of Statistics (e1071). TU Wien

Fan BJ, Pasquale L, Grosskreutz CL, Rhee D, Chen T, DeAngelis MM, Kim I, del Bono E, Miller JW, Li T, Haines JL, Wiggs JL (2008) DNA sequence variants in the LOXL1 gene are associated with pseudoexfoliation glaucoma in a U.S. clinic-based population with broad ethnic diversity. BMC Med Genet 9:5. doi:1471-2350-9-5 [pii] 10.1186/1471-2350-9-5

Hoh J, Wille A, Ott J (2001) Trimming, weighting, and grouping SNPs in human case–control association studies. Genome Res 11(12):2115–2119. doi:10.1101/gr.204001

Huang P, Qi Y, Xu YS, Liu J, Liao D, Zhang SS, Zhang C (2010) Serum cytokine alteration is associated with optic neuropathy in human primary open angle glaucoma. J Glaucoma 19(5):324–330. doi:10.1097/IJG.0b013e3181b4cac7

Ioannidis JP, Patsopoulos NA, Evangelou E (2007) Heterogeneity in meta-analyses of genome-wide association investigations. PLoS One 2(9):e841. doi:10.1371/journal.pone.0000841

Kwon YH, Fingert JH, Kuehn MH, Alward WL (2009) Primary open-angle glaucoma. N Engl J Med 360(11):1113–1124. doi:360/11/1113 [pii] 10.1056/NEJMra0804630

Lambeck AJ, Crijns AP, Leffers N, Sluiter WJ, ten Hoor KA, Braid M, van der Zee AG, Daemen T, Nijman HW, Kast WM (2007) Serum cytokine profiling as a diagnostic and prognostic tool in ovarian cancer: a potential role for interleukin 7. Clin Cancer Res 13(8):2385–2391. doi:13/8/2385 [pii] 10.1158/1078-0432.CCR-06-1828

Listgarten J, Damaraju S, Poulin B, Cook L, Dufour J, Driga A, Mackey J, Wishart D, Greiner R, Zanke B (2004) Predictive models for breast cancer susceptibility from multiple single nucleotide polymorphisms. Clin Cancer Res 10(8):2725–2737

Mabuchi F, Sakurada Y, Kashiwagi K, Yamagata Z, Iijima H, Tsukahara S (2008) Lysyl oxidase-like 1 gene polymorphisms in Japanese patients with primary open angle glaucoma and exfoliation syndrome. Mol Vis 14:1303–1308

McKinney BA, Reif DM, Rock MT, Edwards KM, Kingsmore SF, Moore JH, Crowe JE Jr (2006) Cytokine expression patterns associated with systemic adverse events following smallpox immunization. J Infect Dis 194(4):444–453. doi:JID36092 [pii] 10.1086/505503

Meguro A, Inoko H, Ota M, Mizuki N, Bahram S (2010) Genome-wide association study of normal tension glaucoma: common variants in SRBD1 and ELOVL5 contribute to disease susceptibility. Ophthalmology 117(7):1331–1338. doi: S0161-6420(09)01404-3 [pii] 10.1016/j.ophtha.2009.12.001

Nakano M, Ikeda Y, Taniguchi T, Yagi T, Fuwa M, Omi N, Tokuda Y, Tanaka M, Yoshii K, Kageyama M, Naruse S, Matsuda A, Mori K, Kinoshita S, Tashiro K (2009) Three susceptible loci associated with primary open-angle glaucoma identified by genome-wide association study in a Japanese population. Proc Natl Acad Sci U S A 106(31):12838–12842. doi:0906397106 [pii] 10.1073/pnas.0906397106

Nakano M, Ikeda Y, Tokuda Y, Fuwa M, Omi N, Ueno M, Imai K, Adachi H, Kageyama M, Mori K, Kinoshita S, Tashiro K (2012) Common Variants in CDKN2B-AS1 Associated with Optic-Nerve Vulnerability of Glaucoma Identified by Genome-Wide Association Studies in Japanese. PLoS One 7(3): e33389. doi:10.1371/journal.pone.0033389 PONE-D-11-17292 [pii]

Nelson MR, Kardia SL, Ferrell RE, Sing CF (2001) A combinatorial partitioning method to identify multilocus genotypic partitions that predict quantitative trait variation. Genome Res 11(3):458–470. doi:10.1101/gr.172901

Price AL, Patterson NJ, Plenge RM, Weinblatt ME, Shadick NA, Reich D (2006) Principal components analysis corrects for stratification in genome-wide association studies. Nat Genet 38(8):904–909. doi:ng1847 [pii] 10.1038/ng1847

R Development Core Team (2011) R: A Language and Environment for Statistical Computing

Ray K, Mookherjee S (2009) Molecular complexity of primary open angle glaucoma: current concepts. J Genet 88(4):451–467

Ray S, Britschgi M, Herbert C, Takeda-Uchimura Y, Boxer A, Blennow K, Friedman LF, Galasko DR, Jutel M, Karydas A, Kaye JA, Leszek J, Miller BL, Minthon L, Quinn JF, Rabinovici GD, Robinson WH, Sabbagh MN, So YT, Sparks DL, Tabaton M, Tinklenberg J, Yesavage JA, Tibshirani R, Wyss-Coray T (2007) Classification and prediction of clinical Alzheimer's diagnosis based on plasma signaling proteins. Nat Med 13(11):1359–1362. doi:nm1653 [pii] 10.1038/nm1653

Relton CL, Wilding CS, Pearce MS, Laffling AJ, Jonas PA, Lynch SA, Tawn EJ, Burn J (2004) Gene-gene interaction in folate-related genes and risk of neural tube defects in a UK population. J Med Genet 41(4):256–260

Ritchie MD, Hahn LW, Roodi N, Bailey LR, Dupont WD, Parl FF, Moore JH (2001) Multifactor-dimensionality reduction reveals high-order interactions among estrogen-metabolism genes in sporadic breast cancer. Am J Hum Genet 69(1):138–147. doi:S0002-9297(07)61453-0 [pii] 10.1086/321276

Rojas J, Fernandez I, Pastor JC, Garcia-Gutierrez MT, Sanabria RM, Brion M, Sobrino B, Manzanas L, Giraldo A, Rodriguez-de la Rua E, Carracedo A (2009) Development of predictive models of proliferative vitreoretinopathy based on genetic variables: the Retina 4 project. Invest Ophthalmol Vis Sci 50(5):2384–2390. doi: iovs.08-2670 [pii] 10.1167/iovs.08-2670

Seddon JM, Reynolds R, Maller J, Fagerness JA, Daly MJ, Rosner B (2009) Prediction model for prevalence and incidence of advanced age-related macular degeneration based on genetic, demographic, and environmental variables. Invest Ophthalmol Vis Sci 50(5):2044–2053. doi:iovs.08-3064 [pii] 10.1167/iovs.08-3064

Sengur A (2012) Support vector machine ensembles for intelligent diagnosis of valvular heart disease. J Med Syst 36(4):2649–2655. doi:10.1007/s10916-011-9740-z

Schwender H, Bowers K, Fallin MD, Ruczinski I (2011) Importance measures for epistatic interactions in case-parent trios. Ann Hum Genet 75(1):122–132. doi:10.1111/j.1469-1809.2010.00623.x

Tezel G (2011) The immune response in glaucoma: a perspective on the roles of oxidative stress. Exp Eye Res 93(2):178–186. doi:S0014-4835(10)00220-4 [pii] 10.1016/j.exer.2010.07.009

Thorleifsson G, Magnusson KP, Sulem P, Walters GB, Gudbjartsson DF, Stefansson H, Jonsson T, Jonasdottir A, Stefansdottir G, Masson G, Hardarson GA, Petursson H, Arnarsson A, Motallebipour M, Wallerman O, Wadelius C, Gulcher JR, Thorsteinsdottir U, Kong A, Jonasson F, Stefansson K (2007) Common sequence variants in the LOXL1 gene confer susceptibility to exfoliation glaucoma. Science 317(5843):1397–1400. doi:1146554 [pii] 10.1126/science.1146554

Thorleifsson G, Walters GB, Hewitt AW, Masson G, Helgason A, DeWan A, Sigurdsson A, Jonasdottir A, Gudjonsson SA, Magnusson KP, Stefansson H, Lam DS, Tam PO, Gudmundsdottir GJ, Southgate L, Burdon KP, Gottfredsdottir MS, Aldred MA, Mitchell P, St Clair D, Collier DA, Tang N, Sveinsson O, Macgregor S, Martin NG, Cree AJ, Gibson J, Macleod A, Jacob A, Ennis S, Young TL, Chan JC, Karwatowski WS, Hammond CJ, Thordarson K, Zhang M, Wadelius C, Lotery AJ, Trembath RC, Pang CP, Hoh J, Craig JE, Kong A, Mackey DA, Jonasson F, Thorsteinsdottir U, Stefansson K (2010) Common variants near CAV1 and CAV2 are associated with primary open-angle glaucoma. Nat Genet 42(10):906–909. doi:ng.661 [pii] 10.1038/ng.661

Wang CH, Liu BJ, Wu LS (2012) The Association Forecasting of 13 Variants Within Seven Asthma Susceptibility Genes on 3 Serum IgE Groups in Taiwanese Population by Integrating of Adaptive Neuro-fuzzy Inference System (ANFIS) and Classification Analysis Methods. J Med Syst 36(1):175–185. doi:10.1007/s10916-010-9457-4

Williams SE, Whigham BT, Liu Y, Carmichael TR, Qin X, Schmidt S, Ramsay M, Hauser MA, Allingham RR (2010) Major LOXL1 risk allele is reversed in exfoliation glaucoma in a black South African population. Mol Vis 16:705–712

Yang J, Yang P, Tezel G, Patil RV, Hernandez MR, Wax MB (2001) Induction of HLA-DR expression in human lamina cribrosa astrocytes by cytokines and simulated ischemia. Invest Ophthalmol Vis Sci 42(2):365–371

doi:10.1186/2193-1801-1-41
**Cite this article as:** Tokuda *et al.*: An approach to predict the risk of glaucoma development by integrating different attribute data. *SpringerPlus* 2012 **1**:41.

*The American Journal of Pathology, Vol. 181, No. 6, December 2012*

*http://dx.doi.org/10.1016/j.ajpath.2012.08.023*

*Vascular Biology, Atherosclerosis, and Endothelium Biology*

# Topical Simvastatin Accelerates Wound Healing in Diabetes by Enhancing Angiogenesis and Lymphangiogenesis

Jun Asai,* Hideya Takenaka,* Satoshi Hirakawa,† Jun-ichi Sakabe,† Asami Hagura,* Saburo Kishimoto,* Kazuichi Maruyama,‡ Kentaro Kajiya,§ Shigeru Kinoshita,‡ Yoshiki Tokura,† and Norito Katoh*

*From the Departments of Dermatology* and Ophthalmology,‡ Graduate School of Medical Science, Kyoto Prefectural University of Medicine, Kyoto; the Department of Dermatology,† Hamamatsu University School of Medicine, Hamamatsu; and the Shiseido Innovative Science Research Center,§ Yokohama, Japan*

**Impaired wound healing is a major complication of diabetes. Recent studies have reported reduced lymphangiogenesis and angiogenesis during diabetic wound healing, which are thought to be new therapeutic targets. Statins have effects beyond cholesterol reduction and can stimulate angiogenesis when used systemically. However, the effects of topically applied statins on wound healing have not been well investigated. The present study tested the hypothesis that topical application of simvastatin would promote lymphangiogenesis and angiogenesis during wound healing in genetically diabetic mice. A full-thickness skin wound was generated on the back of the diabetic mice and treated with simvastatin or vehicle topically. Simvastatin administration resulted in significant acceleration of wound recovery, which was notable for increases in both angiogenesis and lymphangiogenesis. Furthermore, simvastatin promoted infiltration of macrophages, which produced vascular endothelial growth factor C in granulation tissues. *In vitro*, simvastatin directly promoted capillary morphogenesis and exerted an antiapoptotic effect on lymphatic endothelial cells. These results suggest that the favorable effects of simvastatin on lymphangiogenesis are due to both a direct influence on lymphatics and indirect effects via macrophages homing to the wound. In conclusion, a simple strategy of topically applied simvastatin may have significant therapeutic potential for enhanced wound healing in patients with impaired microcirculation such as that in diabetes.** *(Am J Pathol 2012, 181:2217–2224; http://dx.doi.org/10.1016/j.ajpath.2012.08.023)*

Delayed wound healing is a major complication of diabetes and is caused by increased apoptosis, delayed cellular infiltration, reduced angiogenesis, and decreased formation and organization of collagen fibers.[1–3] Impaired lymphangiogenesis has also recently been established as a major factor in diabetic refractory wound healing.[4,5] The functions of lymphatic vessels in wounds are to drain the protein-rich lymph from the extracellular space, to maintain normal tissue pressure, and to mediate the immune response.[6,7] Delayed wound healing, such as that seen in infections, appears to result from persistent edema and delayed removal of debris and inflammatory cells due to reduced lymphatic development.[8]

Statins are HMG-CoA (5-hydroxy-3-methylglutaryl-coenzyme A) reductase inhibitors that are primarily used to lower circulating cholesterol levels. In addition, statins have been found to protect against ischemic injury and stimulate angiogenesis in normocholesterolemic animals.[9–11] This angiogenic effect is partially mediated by direct regulation of proliferation of endothelial cells and capillary morphogenesis via the Akt/PI3K pathway.[11] Simvastatin has been found to enhance vascular endothelial growth factor (VEGF) production and improve wound healing in an experimental model of diabetes,[12] and nitropravastatin stimulates reparative neovascularization and improves recovery from limb ischemia in type 1 diabetic mice.[13] However, systemic administration at an extremely high dose was used to obtain angiogenic effects in

Supported by grants from the Ministry of Education, Culture, Sports, Science and Technology of Japan.

Accepted for publication August 15, 2012.

CME Disclosure: The authors of this article and the planning committee members and staff have no relevant financial relationships with commercial interest to disclose.

Supplemental material for this article can be found at *http://ajp.amjapathol.org* or at *http://dx.doi.org/10.1016/j.ajpath.2012.08.023*.

Address reprint requests to Jun Asai, M.D., Ph.D., Department of Dermatology, Graduate School of Medical Science, Kyoto Prefectural University of Medicine, 465 Hirokoji, Kawaramachi, Kamigyo-Ku, Kyoto, 602-8566, Japan. E-mail: jasai@koto.kpu-m.ac.jp.

these studies, and this is inapplicable for clinical use as an angiogenic drug in patients with ischemic disorders. However, topical application of statins with avoidance of systemic adverse effects may be useful for cutaneous wound healing, in which angiogenesis plays a pivotal role.[14] The lymphangiogenic effects of statins have not been widely investigated. In this study, we evaluated the effects of topical simvastatin on angiogenesis and lymphangiogenesis in a mouse model of impaired diabetic wound healing.

## Materials and Methods

### Animals

Genetically diabetic C57BLKS/J-m+/+*Lepr*$^{db}$ mice (db/db mice) were obtained from Clea Japan, Inc. (Tokyo, Japan). All procedures were performed in accordance with the guidelines of the Animal Care and Use Committees of Kyoto Prefectural University of Medicine.

### Creation of Wounds

Mice were between 6 and 10 weeks old at the time of the study. Wounds were generated as described previously.[15–17] In brief, after induction of deep anesthesia by i.p. injection of sodium pentobarbital (160 mg/kg), full-thickness, excisional skin wounds using 8-mm skin biopsy punches were made on the backs of mice, with one wound generated in each mouse. Each wound was covered with a semipermeable polyurethane dressing (OpSite; Smith and Nephew, Massillon, OH) after topical application of simvastatin (Calbiochem, La Jolla, CA) in petroleum jelly (a mixture of 5 mg of simvastatin and 995 mg of jelly) or vehicle (petroleum jelly alone). Simvastatin in petroleum jelly (10 mg of the mixture containing 50 $\mu$g of simvastatin) or vehicle were applied to the wound on days 0, 4, 7, and 10 after creation of the wound.

### Monitoring of Wound Healing

A total of 5 db/db mice were used at each time point. Wound healing was monitored by taking pictures with a digital camera (Nikon Coolpix 995; Nikon, Tokyo, Japan) on days 0, 4, 7, and 14 after wound creation. Images were analyzed using ImageJ software version 1.46 (NIH, Bethesda, MD)[18] by tracing the wound margin with a high-resolution computer mouse and calculating the pixel area. Wound closure was calculated as follows: Percentage Closed = [(Area on Day 0 − Open Area on Final Day)/Area on Day 0] × 100, as described previously.[15] The areas of the wounds were compared with Student's *t*-test with $P < 0.05$ taken to indicate a significant difference.

### Histologic Score

A histologic score was assigned in a masked manner as described previously.[15] Briefly, each specimen received a score of 1 to 12 as follows: 1 to 3, none to minimal cell accumulation and granulation tissue or epithelial migration; 4 to 6, thin, immature granulation dominated by inflammatory cells but with few fibroblasts, capillaries, or collagen deposition and minimal epithelial migration; 7 to 9, moderately thick granulation tissue, ranging from mainly inflammatory cells to more fibroblasts and collagen deposition; and 10 to 12, thick, vascular granulation tissue dominated by fibroblasts and extensive collagen deposition.

### Evaluation of Wound Angiogenesis and Lymphangiogenesis

Sections were stained with rat anti-CD31 antibody (1:100) (BD Biosciences, San Jose, CA) or rabbit anti-LYVE-1 antibody (Upstate, Lake Placid, NY). Green fluorescence was generated by labeling with fluorescein isothiocyanate (FITC)–streptavidin (Vector Laboratories, Burlingame, CA) and biotinylated anti-rat or anti-rabbit antibody (both Vector Laboratories). Wound angiogenesis or lymphangiogenesis was analyzed by calculating the percentage of fluorescent area.[16,19] Briefly, for each slide, an image of the granulation tissue at the wound margin was captured. ImageJ software was used to quantitate the fluorescence intensity. The mean percentage of fluorescent pixels of five images served as an index of the angiogenic or lymphangiogenic response.

### Evaluation of Macrophage Number, Phenotype, and VEGF-C Expression in Granulation Tissue

Sections of wounds were stained with rat anti-F4/80 antibody (Invitrogen, Carlsbad, CA). Labeling with F4/80 was visualized with Cy3-conjugated anti-rat antibody (Vector Laboratories). Ten granulation tissue fields (two sections from each animal) were selected, and F4/80-positive cells were counted.[16] VEGF-C expression was evaluated using goat anti-VEGF-C antibody (Santa Cruz Biotechnology, Santa Cruz, CA) and FITC-conjugated anti-goat antibody (Vector Laboratories). To determine the phenotype of infiltrating macrophages, IL-13 and tumor necrosis factor (TNF) $\alpha$ expression was evaluated using goat anti-IL-13 antibody and goat anti-TNF-$\alpha$ antibody (Santa Cruz Biotechnology), respectively, and FITC-conjugated anti-goat antibody. F4/80-positive TNF-$\alpha$–positive cells were defined as an M1 phenotype and F4/80-positive IL-13–positive cells as an M2 phenotype. In each slide, F4/80-positive cells, F4/80-positive TNF-$\alpha$–positive cells, and F4/80-positive IL-13–positive cells were counted, and percentages of TNF-$\alpha$–positive macrophages and IL-13–positive macrophages were evaluated. The mean percentages of TNF-$\alpha$–positive macrophages and IL-13–positive macrophages in five images were used as indexes of the M1 and M2 phenotypes, respectively.

### RNA Isolation, cDNA Synthesis, and Quantitative RT-PCR

Tissue sections obtained in RNAlater (Ambion, Paisley, UK) were processed for RNA isolation, cDNA synthesis, and quantitative RT-PCR.[16] VEGF-C, fibroblast growth factor 2, endothelial nitric oxide synthase, stromal cell-derived factor 1$\alpha$, and platelet-derived growth factor $\beta$ gene expression levels were normalized based on the level of an internal

reference gene, 18S. The primers used in the study were obtained from QIAGEN (Dűsseldorf, Germany).

### *Cell Culture*

Primary human lymphatic endothelial cells (LECs) were collected as previously described.[20] LECs were cultured at 37°C in 5% $CO_2$ in endothelial cell basal medium 2 (Lonza, Walkersville, MD) supplemented with 5% fetal bovine serum, human VEGF-A, human fibroblast growth factor 2, human epidermal growth factor, insulin-like growth factor 1, and ascorbic acid. Each experiment was conducted at least three times, with similar results. A representative experiment is shown.

### *Western Blot Analysis*

Cells were lysed with RIPA buffer (Invitrogen) and sonicated. After sonication, cell lysates were centrifuged at 15,400 × *g* for 20 minutes at 4°C, and the supernatants were collected into fresh tubes. Then 4× SDS sample buffer with 0.1 mol/L dithiothreitol was added to samples. Samples were boiled for 5 minutes at 95°C, and 20-μg extracts were separated by 10% SDS-PAGE and electroblotted onto polyvinylidene difluoride membranes for 2 hours at 180 mA. The membranes were incubated with rabbit anti-human Akt (pan) (C67E7) monoclonal antibody (Cell Signaling Technology, Danvers, MA), rabbit anti-human phospho-Akt (Ser473) (D9E) monoclonal antibody (Cell Signaling Technology), or mouse anti-GAPDH monoclonal antibody (Santa Cruz Biotechnology) and detected with horseradish peroxidase–conjugated goat anti-rabbit IgG (Bio-Rad, Hercules, CA) or horseradish peroxidase–conjugated goat anti-mouse IgG (Bio-Rad). Immunoblots were visualized using an ECL Plus Western Blotting Detection Reagents Kit (GE Healthcare, Little Chalfont, Buckinghamshire, UK) according to the manufacturer protocol.

### *Chord Formation Assay*

LECs were used in a chord formation assay.[21] An aliquot (100 μL) of growth factor–depleted Matrigel (Becton Dickinson, Bedford, MA) was added to a 24-well dish and allowed to gel for 30 minutes at 37°C. LECs were seeded at $5 \times 10^4$ cells/mL in 500 μL of endothelial cell basal medium 2 containing 3% fetal bovine serum. Cells were cultured in the absence or presence of various doses of simvastatin (Calbiochem, Darmstadt, Germany) with or without pretreatment with a PI3 kinase inhibitor, LY294002 (50 μmol/L) (ENZO Life Sciences, Plymouth Meeting, PA), the mTOR/raptor inhibitor rapamycin (100 nmol/L) (Merck Millipore, Darmstadt, Germany), or the PI3K/mTOR inhibitor wortmannin-rapamycin (100 nmol/L) (Cayman Chemical, Ann Arbor, MI) for 30 minutes. Chord formation was monitored for 24 hours. Digital pictures were taken using a spot image analysis system, and the total length of the chord-like structures at 12 hours was outlined and measured using ImageJ software.

### *Proliferation Assay*

The proliferative activity of cells treated with simvastatin was examined using a CellTiter 96 nonradioactive cell proliferation assay (Promega, Madison, WI). Briefly, subconfluent cells (5000 cells per well) were reseeded on 96-well, flat-bottomed plates with 100 μL of growth media. The cells were treated with simvastatin and incubated for 48 hours at 37°C. Absorbance at 570 nm was recorded using a 96-well enzyme-linked immunosorbent assay (ELISA) plate reader.

### *Apoptosis Assay*

An apoptosis assay was performed using a DeadEnd Fluorometric TUNEL System (Promega). Briefly, LECs were plated on chamber slides and placed in medium. Cells were stimulated by simvastatin and incubated for 24 hours with medium containing 400 μmol/L $H_2O_2$. To quantify apoptosis, 400 nuclei from random microscopic fields were analyzed by an observer masked to the treatment groups. The number of apoptotic cells was expressed as a percentage of the total cell count.

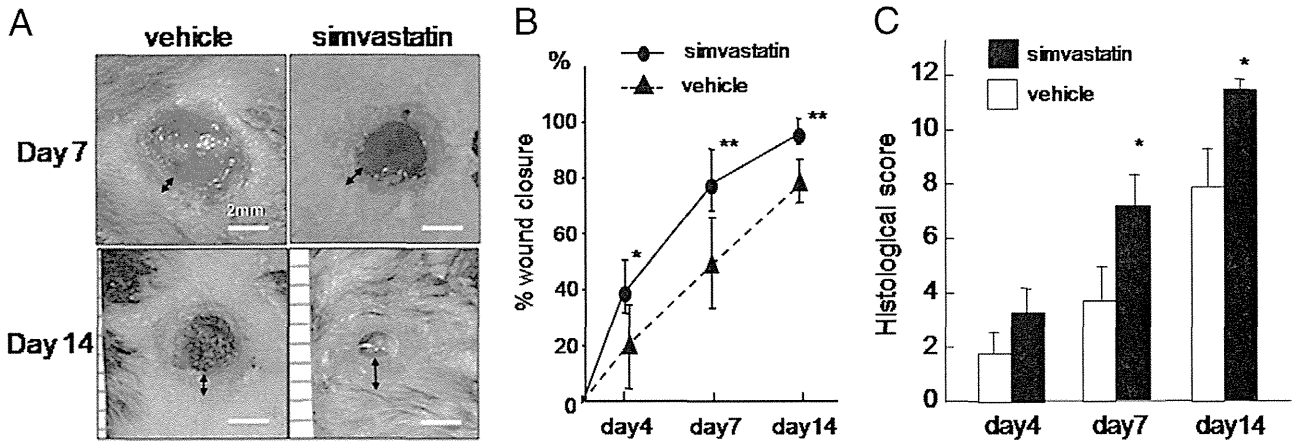


**Figure 1.** Effects of topical simvastatin on wound closure and histologic score in db/db mice. **A:** Representative macroscopic views of wounds after different treatments and periods. Scale bar = 2 mm. **Arrows** indicate the epithelialized range. **B:** Wound closure was measured on days 4, 7, and 14. $^*P < 0.05$, $^{**}P < 0.001$ versus vehicle ($n = 5$ in each group). **C:** Histologic scores for days 4, 7, and 14, quantified as described in *Materials and Methods*. Higher histologic scores indicate a greater extent of wound healing. $^*P < 0.05$ versus vehicle ($n = 5$ in each group).

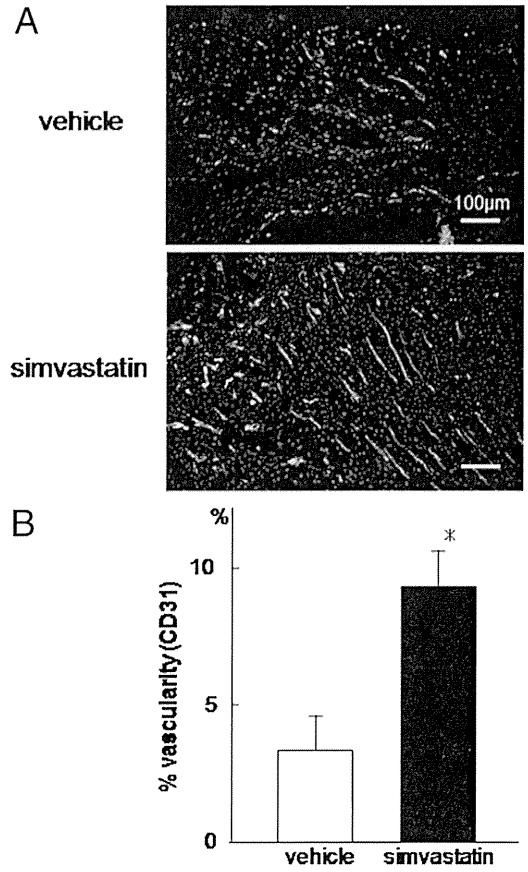


**Figure 2.** Effects of simvastatin on vascularity in granulation tissues at the wound margin in db/db mice. **A:** Neovascularization at the wound margin in simvastatin- or vehicle-treated diabetic mice after 14 days. Original magnification, ×100. Scale bar = 100 μm. Green and blue fluorescence corresponds to CD31-positive newly formed blood vessels and DAPI-labeled nuclei, respectively. **B:** Percentage of vascularity, quantified as described in *Materials and Methods*. *$P < 0.001$ versus vehicle ($n = 5$ in each group).

### *Statistical Analysis*

All results are presented as mean ± SEM. Statistical comparisons between two groups were performed by Student's *t*-test. Multiple groups were analyzed by one-way analysis of variance followed by appropriate post hoc tests to determine statistical significance. $P < 0.05$ was considered significant. All *in vitro* experiments were performed at least in triplicate.

## *Results*

### *Simvastatin Accelerates Wound Healing in Diabetic Mice*

Wound areas on days 7 and 14 in simvastatin- or vehicle-treated diabetic mice are shown in Figure 1A. On day 14, simvastatin-treated wounds had more than 90% epithelialization, whereas <80% of the wound was epithelialized in the vehicle-treated group (Figure 1B). Simvastatin treatment resulted in significantly smaller wound areas after 4, 7, and 14 days. The difference in percentage of wound closure reached a maximum on day 7 (simvastatin versus control: 79.26% ± 11.09% versus 52.45% ± 16.81%; $P < 0.001$). The histologic score reflects the degree of maturation of granulation tissue, including inflammation, collagen deposition, and reepithelialization, in addition to neovascularization; therefore, higher histologic scores reflect a greater extent of wound healing. The histologic scores for wounds treated with simvastatin were significantly higher than those in the vehicle-treated group (day 4: 3.6 ± 0.70 versus 1.9 ± 0.73; day 7: 7.3 ± 0.94 versus 3.7 ± 0.94, $P < 0.01$; day 14: 11.6 ± 0.51 versus 8.0 ± 1.15, $P < 0.01$)(Figure 1C).

### *Simvastatin Promotes Both Angiogenesis and Lymphangiogenesis*

Wound angiogenesis was analyzed by immunostaining of an endothelial cell–specific marker, CD31, in 10-μm frozen sections to visualize neovascularization. Figure 2A shows neovascularization at the margin in simvastatin- or vehicle-treated wounds in diabetic mice on day 14. A few small vessels were seen at the wound margin in the vehicle-treated group, whereas large numbers of vessels were growing toward the center of the wound in the

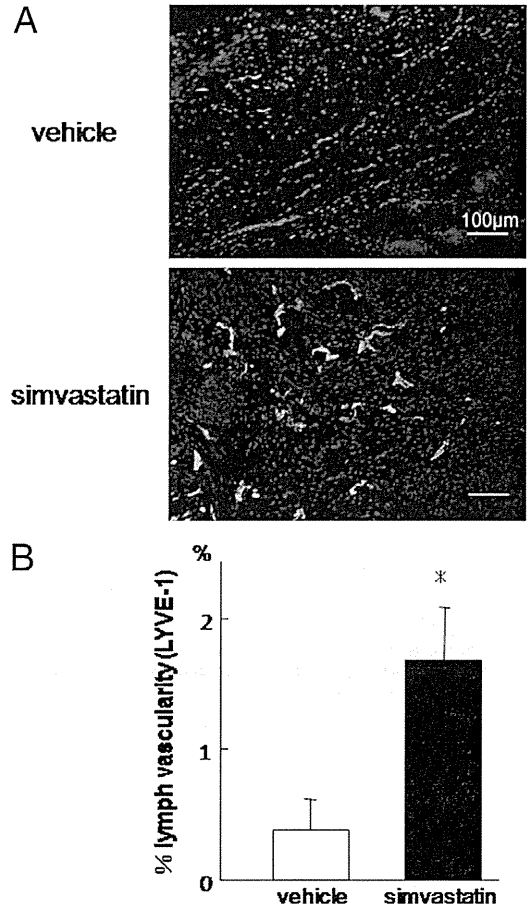


**Figure 3.** Effects of simvastatin on lymphangiogenesis in granulation tissues at the wound margin in db/db mice. **A:** Lymphangiogenesis at the wound margin in simvastatin- or vehicle-treated diabetic mice after 14 days. Original magnification, ×100. Scale bar =100 μm. Green and blue fluorescence corresponds to LYVE-1–positive newly formed lymphatic vessels and DAPI-labeled nuclei, respectively. **B:** Percentage of lymphatic vascularity, quantified as described in *Materials and Methods*. *$P < 0.001$ versus vehicle ($n = 5$ in each group).

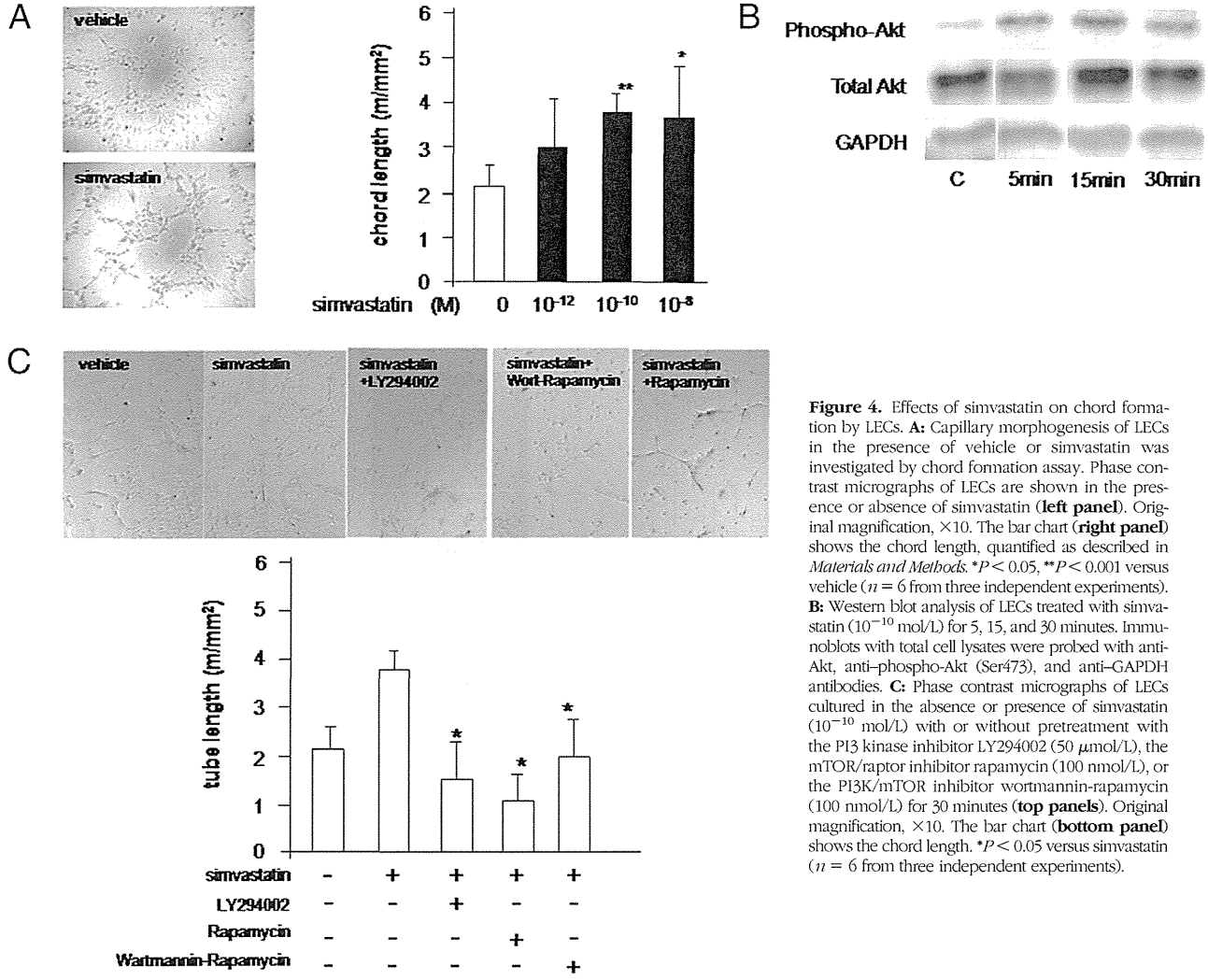


**Figure 4.** Effects of simvastatin on chord formation by LECs. **A:** Capillary morphogenesis of LECs in the presence of vehicle or simvastatin was investigated by chord formation assay. Phase contrast micrographs of LECs are shown in the presence or absence of simvastatin (**left panel**). Original magnification, ×10. The bar chart (**right panel**) shows the chord length, quantified as described in *Materials and Methods*. $^{*}P < 0.05$, $^{**}P < 0.001$ versus vehicle ($n = 6$ from three independent experiments). **B:** Western blot analysis of LECs treated with simvastatin ($10^{-10}$ mol/L) for 5, 15, and 30 minutes. Immunoblots with total cell lysates were probed with anti-Akt, anti–phospho-Akt (Ser473), and anti–GAPDH antibodies. **C:** Phase contrast micrographs of LECs cultured in the absence or presence of simvastatin ($10^{-10}$ mol/L) with or without pretreatment with the PI3 kinase inhibitor LY294002 (50 μmol/L), the mTOR/raptor inhibitor rapamycin (100 nmol/L), or the PI3K/mTOR inhibitor wortmannin-rapamycin (100 nmol/L) for 30 minutes (**top panels**). Original magnification, ×10. The bar chart (**bottom panel**) shows the chord length. $^{*}P < 0.05$ versus simvastatin ($n = 6$ from three independent experiments).

simvastatin group. Simvastatin significantly enhanced wound vascularity based on image analysis of the percentage of the fluorescent area (9.29% ± 1.29% versus 3.25% ± 1.33%; $P < 0.001$)(Figure 2B). Wound lymphangiogenesis was analyzed by immunostaining of a LEC-specific marker, LYVE-1, in 10-μm frozen sections. Figure 3A shows new lymphatic vessels at the margin of simvastatin- or vehicle-treated wounds in diabetic mice on day 14. Wound lymphatic vascularity was significantly enhanced by simvastatin (percentage of fluorescent area: 1.72% ± 0.460% versus 0.395% ± 0.260%; $P < 0.001$) (Figure 3B). New vessels and lymphatics in granulation tissue in both groups were not covered with α-smooth muscle actin–positive mural cells (see Supplemental Figure S1 at *http://ajp.amjpathol.org*).

## *Simvastatin Induces Capillary Morphogenesis of LECs and Has an Antiapoptotic Effect but Does Not Induce Proliferation*

To characterize the effects of simvastatin on lymphangiogenesis, we performed a chord formation assay in primary human LECs *in vitro*. Treatment with simvastatin promoted LEC chord formation in a dose-dependent manner (Figure 4A). This effect was significantly blocked by the PI3 kinase inhibitor LY294002, the mTOR inhibitor rapamycin, and the PI3/mTOR inhibitor wortmannin-rapamycin ($P < 0.05$)(Figure 4C). The proliferative and antiapoptotic effects of simvastatin on LECs were also examined because these are major effects of simvastatin in vascular endothelial cells. Simvastatin did not promote LEC proliferation, even at higher concentrations, and seemed to be slightly cytotoxic at $10^{-6}$ mol/L and $10^{-5}$ mol/L (Figure 5A). However, simvastatin treatment resulted in significant inhibition of $H_2O_2$-induced apoptosis compared with controls (Figure 5B).

## *Simvastatin Promotes Macrophage Infiltration and VEGF-C Production in Wounds*

The number of macrophages in granulation tissues was evaluated in wounds on day 7. This timing was chosen because reepithelialization was almost complete on day 14 in simvastatin-treated wounds, and inflammatory cells had already diminished. The number of macrophages in simvastatin-treated wounds on day 7 was significantly

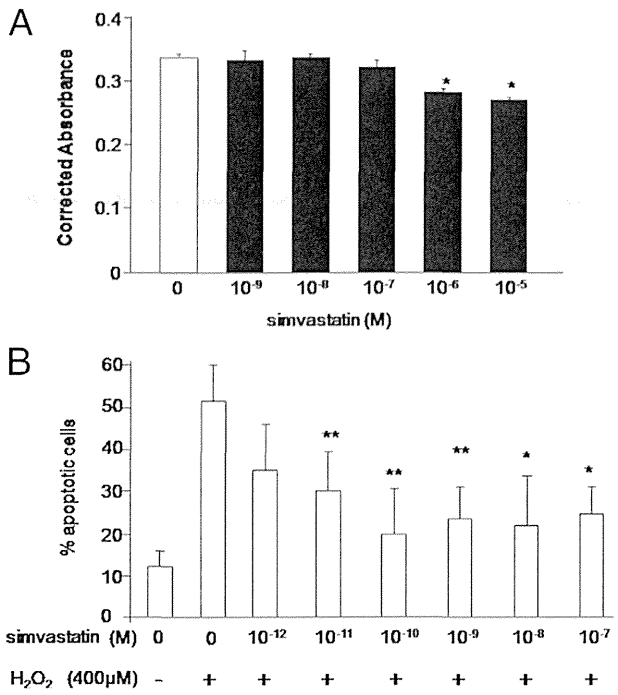


**Figure 5.** Effects of simvastatin on proliferation and apoptosis of LECs. **A:** Cell proliferation of LECs was investigated by MTS assay. Subconfluent cells (5000 cells per well) were reseeded on 96-well, flat-bottomed plates with 100 μL of growth media. The cells were treated with simvastatin and incubated for 48 hours at 37°C. Absorbance at 570 nm was recorded using a 96-well ELSIA plate reader. Quantification was performed as described in *Materials and Methods*. $^*P < 0.05$ versus vehicle ($n = 8$ from three independent experiments). **B:** Cell apoptosis in LECs was investigated by TUNEL assay. LECs were plated on chamber slides and placed in medium. Cells were stimulated by simvastatin and incubated for 24 hours with medium containing 400 μmol/L $H_2O_2$. Quantification of apoptotic cells was performed as described in *Materials and Methods*. $^*P < 0.05$, $^{**}P < 0.01$ versus $H_2O_2$ treatment ($n = 3$ from three independent experiments).

greater than that in controls (Figure 6, A and B). Most of the macrophages in the simvastatin-treated group expressed the M2 marker, IL-13, rather than the M1 marker, TNF-α, whereas most macrophages in the vehicle-treated group expressed TNF-α rather than IL-13 (Figure 6, C–F). The macrophages in the simvastatin-treated group produced VEGF-C (Figure 7A), and VEGF-C expression was significantly up-regulated in simvastatin-treated wounds compared with controls (Figure 7B). Other proangiogenic mediators in wound granulation tissue were evaluated by real-time PCR. Platelet-derived growth factor β, endothelial nitric oxide synthase, and fibroblast growth factor 2 were significantly up-regulated by simvastatin stimulation (see Supplemental Figure S2 at *http://ajp.amjpathol.org*).

## Discussion

In this study, we found that topical application of simvastatin accelerated diabetic wound healing via promotion of angiogenesis and lymphangiogenesis. Many studies have reported that statins, including simvastatin, have strong angiogenic effects on vascular endothelial cells or placental stem cells and that these effects are mainly mediated by the PI3-kinase/Akt pathway,[11,22,23] although we note that other findings have also been reported[24] Consistent with these reports, abundant neovascularization and proangiogenic growth factors were observed in wounds treated with topical simvastatin in our *in vivo* study. Statins were originally introduced as systemic antihyperlipidemic drugs; however, a recent study has shown the value of topical simvastatin.[14] An advantage of topical application is that a suitable concentration of simvastatin can be applied without a risk of serious systemic adverse effects, such as rhabdomyolysis. Our results suggest that topical application of simvastatin could be a

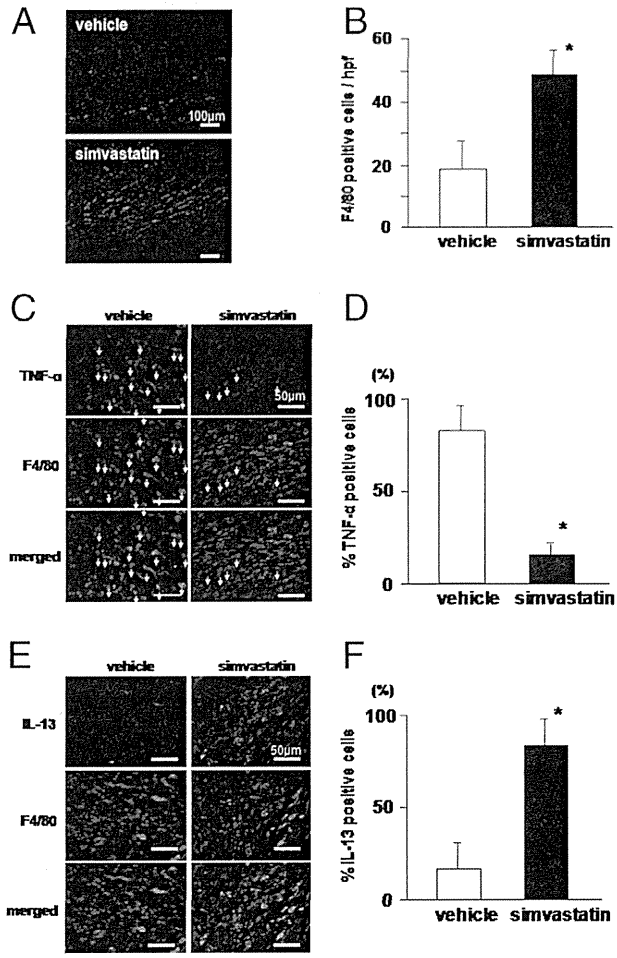


**Figure 6.** Effects of simvastatin on macrophage infiltration and phenotype in granulation tissue. **A:** Representative photomicrographs of the immunostained wound edge at 7 days after wound creation. Red fluorescence corresponds to F4/80-positive macrophages. Scale bar = 100 μm. **B:** The macrophage count, quantified as described in *Materials and Methods*. $^*P < 0.05$ versus vehicle ($n = 5$). **C:** Representative photomicrographs of the immunodetection of TNF-α and F4/80 in histologic sections from vehicle- or simvastatin-treated wounds (original magnification ×400). Scale bar = 50 μm. Green and red fluorescence corresponds to TNF-α–positive cells and F4/80-positive macrophages, respectively. Yellow indicates TNF-α–producing M1 phenotype macrophages (**white arrows**). **D:** Quantification of percentage of TNF-α–positive macrophages, as described in *Materials and Methods*. $^*P < 0.001$ versus vehicle ($n = 5$ in each group). **E:** Representative photomicrographs of immunodetection of IL-13 and F4/80 in histologic sections from vehicle- or simvastatin-treated wounds (original magnification ×400). Scale bar = 50 μm. Green and red fluorescence correspond to IL-13–positive cells and F4/80-positive macrophages, respectively. Yellow indicates IL-13–producing M2 phenotype macrophages. **F:** Quantification of percentage of IL-13–positive macrophages, as described in *Materials and Methods*. $^*P < 0.001$ versus vehicle ($n = 5$ in each group).

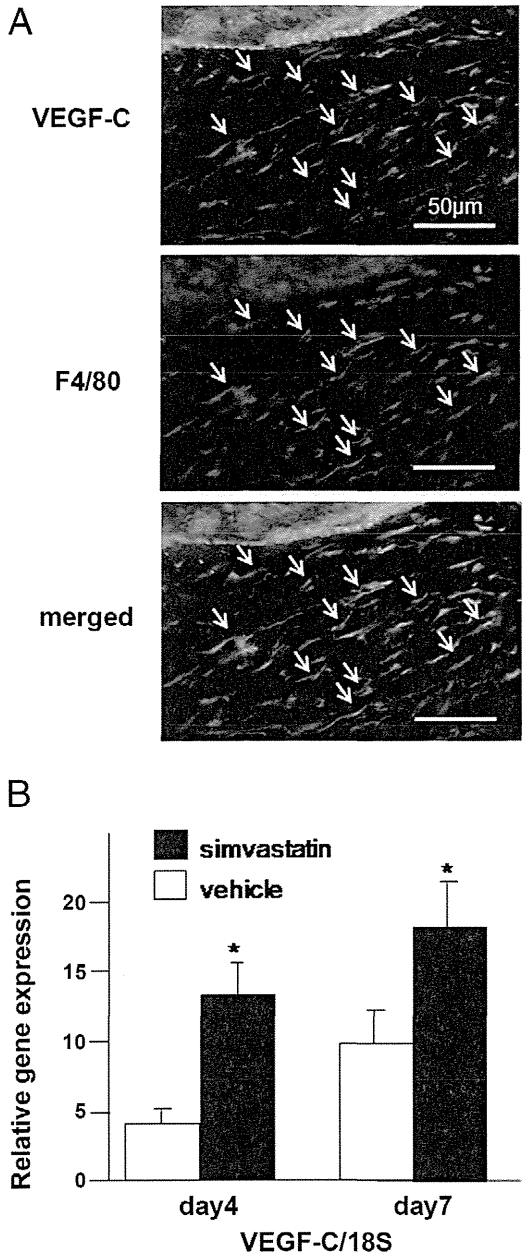


**Figure 7.** VEGF-C expression in granulation tissue. **A:** Representative photomicrographs of the immunostained wound edge treated with simvastatin at 7 days after wound creation. Green and red fluorescence indicates VEGF-C expression and F4/80-positive macrophages, respectively. Original magnification, ×400. **Arrows** indicate double-positive cells. Scale bar = 50 μm. **B:** Quantitative RT-PCR of VEGF-C in wound granulation tissue. Gene expression levels were normalized based on the level of an internal reference gene, 18S. $^*P < 0.05$ versus vehicle ($n = 5$).

new therapeutic strategy for treatment of local ischemic conditions, such as those in patients with diabetic ulcers.

Lymphangiogenesis is a major factor in diabetic refractory wound healing.[4,5] Therefore, we focused on the effects of simvastatin on wound lymphangiogenesis. Recent studies have suggested that several biological functions of LECs are partially regulated by the AKT/PI3K/mTOR pathway.[25,26] Consistent with these observations, capillary morphogenesis of LECs was significantly stimulated by simvastatin as an effect on vascular endothelial cells that was, at least in part, regulated by the AKT/PI3K/mTOR pathway. Our results suggest that the mechanisms underlying the lymphangiogenic effects of simvastatin in LECs might be similar to those for angiogenic effects. These mechanisms include antiapoptosis and promotion of capillary morphogenesis because LECs develop from a vascular network in an embryonic stage,[27] and these cells have a similar lineage. However, contrary to our expectation, simvastatin did not promote proliferation of LECs *in vitro*. During the wound healing process, new lymphatics are formed in newly generated granulation tissue, indicating that proliferation of preexisting lymphatic vessels is needed.

Because simvastatin did not promote the proliferation of LECs, we evaluated other possible sources of lymphangiogenic factors. Several reports suggest that infiltrating macrophages contribute to lymphangiogenesis as the major producer of VEGF-C in cutaneous wound healing,[4,5] and therefore we evaluated the effects of simvastatin on macrophages. Macrophages carry VEGF receptor 3, in addition to producing VEGF-C, and thus act as both autocrine and paracrine factors. We have previously reported that healing impairment in diabetes involves reduced lymphangiogenesis and suppressed macrophage function, such as recruitment to inflammatory sites and secretion of growth factors.[5] In this study, the number of infiltrating macrophages in granulation tissue was significantly increased by topical application of simvastatin, and most of these macrophages produced VEGF-C. These observations suggest that simvastatin recovers lymphangiogenic function that is impaired in macrophages under diabetic conditions.

Increased apoptosis is a major concern in wound healing in a diabetic state.[3,28–31] Hyperglycemia induces proinflammatory cytokines, such as TNF-$\alpha$, and oxidative stress, which result in increased apoptosis in diabetes. Our study found that most infiltrating macrophages in diabetic wounds had an M1 proinflammatory phenotype producing abundant TNF-$\alpha$. Simvastatin decreased $H_2O_2$-induced apoptosis in LECs *in vitro* and increased M2 anti-inflammatory phenotype macrophages in granulation tissue *in vivo*. We suggest that this anti-apoptotic effect of simvastatin also plays an important role, in addition to promotion of angiogenesis and lymphangiogenesis.

Increased infiltration of macrophages induced by simvastatin may have further benefits because the histologic scores of diabetic wounds were significantly improved by topical application of simvastatin. The histologic score reflects the degree of maturation of granulation tissue, including inflammation, collagen deposition, and reepithelialization, in addition to neovascularization. Macrophages play a central role in all stages of wound healing and orchestrate the wound healing process[32] by exerting proinflammatory functions and facilitating wound healing during the early stage and stimulating proliferation of fibroblasts, keratinocytes, and endothelial cells in the proliferative stage. Because the main focus of this study was lymphangiogenesis, we did not investigate the effects of simvastatin on reepithelialization or formation of extracellular matrix. This will require further experiments in a future study.

In conclusion, regulation of apoptosis and capillary differentiation are essential for development of functional lymphatics during wound healing. The findings of the present study suggest that topical simvastatin can stimulate lymp-

hangiogenesis directly and indirectly via stimulation of macrophages. Vascular remodeling induced by simvastatin might have therapeutic potential in patients with microvascular dysfunction, such as that in diabetic foot ulcer, a major cause of morbidity in the growing population of patients with diabetes. A future investigation is warranted to determine the potential clinical utility of this approach.

## References

1. Jeffcoate WJ, Harding KG: Diabetic foot ulcers. Lancet 2003, 361: 1545–1551
2. Lerman OZ, Galiano RD, Armour M, Levine JP, Gurtner GC: Cellular dysfunction in the diabetic fibroblast: impairment in migration, vascular endothelial growth factor production, and response to hypoxia. Am J Pathol 2003, 162:303–312
3. Fadini GP, Albiero M, Menegazzo L, Boscaro E, Pagnin E, Iori E, Cosma C, Lapolla A, Pengo V, Stendardo M, Agostini C, Pelicci PG, Giorgio M, Avogaro A: The redox enzyme p66Shc contributes to diabetes and ischemia-induced delay in cutaneous wound healing. Diabetes 2010, 59:2306–2314
4. Saaristo A, Tammela T, Farkkila A, Karkkainen M, Suominen E, Yla-Herttuala S, Alitalo K: Vascular endothelial growth factor-C accelerates diabetic wound healing. Am J Pathol 2006, 169:1080–1087
5. Maruyama K, Asai J, Ii M, Thorne T, Losordo DW, D'Amore PA: Decreased macrophage number and activation lead to reduced lymphatic vessel formation and contribute to impaired diabetic wound healing. Am J Pathol 2007, 170:1178–1191
6. Oliver G, Detmar M: The rediscovery of the lymphatic system: old and new insights into the development and biological function of the lymphatic vasculature. Genes Dev 2002, 16:773–783
7. Witte MH, Bernas MJ, Martin CP, Witte CL: Lymphangiogenesis and lymphangiodysplasia: from molecular to clinical lymphology. Microsc Res Tech 2001, 55:122–145
8. Ji RC: Characteristics of lymphatic endothelial cells in physiological and pathological conditions. Histol Histopathol 2005, 20:155–175
9. Werner N, Nickenig G, Laufs U: Pleiotropic effects of HMG-CoA reductase inhibitors. Basic Res Cardiol 2002, 97:105–116
10. Landmesser U, Engberding N, Bahlmann FH, Schaefer A, Wiencke A, Heineke A, Spiekermann S, Hilfiker-Kleiner D, Templin C, Kotlarz D, Mueller M, Fuchs M, Hornig B, Haller H, Drexler H: Statin-induced improvement of endothelial progenitor cell mobilization, myocardial neovascularization, left ventricular function, and survival after experimental myocardial infarction requires endothelial nitric oxide synthase. Circulation 2004, 110:1933–1939
11. Kureishi Y, Luo Z, Shiojima I, Bialik A, Fulton D, Lefer DJ, Sessa WC, Walsh K: The HMG-CoA reductase inhibitor simvastatin activates the protein kinase Akt and promotes angiogenesis in normocholesterolemic animals. Nat Med 2000, 6:1004–1010
12. Bitto A, Minutoli L, Altavilla D, Polito F, Fiumara T, Marini H, Galeano M, Calo M, Lo Cascio P, Bonaiuto M, Migliorato A, Caputi AP, Squadrito F: Simvastatin enhances VEGF production and ameliorates impaired wound healing in experimental diabetes. Pharmacol Res 2008, 57:159–169
13. Emanueli C, Monopoli A, Kraenkel N, Meloni M, Gadau S, Campesi I, Ongini E, Madeddu P: Nitropravastatin stimulates reparative neovascularisation and improves recovery from limb ischaemia in type-1 diabetic mice. Br J Pharmacol 2007, 150:873–882
14. Otuki MF, Pietrovski EF, Cabrini DA: Topical simvastatin: preclinical evidence for a treatment of skin inflammatory conditions. J Dermatol Sci 2006, 44:45–47
15. Greenhalgh DG, Sprugel KH, Murray MJ, Ross R: PDGF and FGF stimulate wound healing in the genetically diabetic mouse. Am J Pathol 1990, 136:1235–1246
16. Asai J, Takenaka H, Katoh N, Kishimoto S: Dibutyryl cAMP influences endothelial progenitor cell recruitment during wound neovascularization. J Invest Dermatol 2006, 126:1159–1167
17. Asai J, Takenaka H, Kusano KF, Ii M, Luedemann C, Curry C, Eaton E, Iwakura A, Tsutsumi Y, Hamada H, Kishimoto S, Thorne T, Kishore R, Losordo DW: Topical sonic hedgehog gene therapy accelerates wound healing in diabetes by enhancing endothelial progenitor cell-mediated microvascular remodeling. Circulation 2006, 113:2413–2424
18. Abràmoff MD, Magalhães PJ, Ram S: J: image processing with ImageJ. Biophotonics Int 2004, 11:36–42
19. Jacobi J, Jang JJ, Sundram U, Dayoub H, Fajardo LF, Cooke JP: Nicotine accelerates angiogenesis and wound healing in genetically diabetic mice. Am J Pathol 2002, 161:97–104
20. Hirakawa S, Hong YK, Harvey N, Schacht V, Matsuda K, Libermann T, Detmar M: Identification of vascular lineage-specific genes by transcriptional profiling of isolated blood vascular and lymphatic endothelial cells. Am J Pathol 2003, 162:575–586
21. Maruyama K, Ii M, Cursiefen C, Jackson DG, Keino H, Tomita M, Van Rooijen N, Takenaka H, D'Amore PA, Stein-Streilein J, Losordo DW, Streilein JW: Inflammation-induced lymphangiogenesis in the cornea arises from CD11b-positive macrophages. J Clin Invest 2005, 115:2363–2372
22. Nakao T, Shiota M, Tatemoto Y, Izumi Y, Iwao H: Pravastatin induces rat aortic endothelial cell proliferation and migration via activation of PI3K/Akt/mTOR/p70 S6 kinase signaling. J Pharmacol Sci 2007, 105:334–341
23. Cantoni S, Cavallini C, Bianchi F, Bonavita F, Vaccari V, Olivi E, Frascari I, Tassinari R, Valente S, Lionetti V, Ventura C: Rosuvastatin elicits KDR-dependent vasculogenic response of human placental stem cells through PI3K/AKT pathway. Pharmacol Res 2012, 65:275–284
24. Zhao TT, Trinh D, Addison CL, Dimitroulakos J: Lovastatin inhibits VEGFR and AKT activation: synergistic cytotoxicity in combination with VEGFR inhibitors. PLoS One 2010, 5:e12563
25. Luo Y, Liu L, Rogers D, Su W, Odaka Y, Zhou H, Chen W, Shen T, Alexander JS, Huang S: Rapamycin inhibits lymphatic endothelial cell tube formation by downregulating vascular endothelial growth factor receptor 3 protein expression. Neoplasia 2012, 14:228–237
26. Dellinger MT, Brekken RA: Phosphorylation of Akt and ERK1/2 is required for VEGF-A/VEGFR2-induced proliferation and migration of lymphatic endothelium. PLoS One 2011, 6:e28947
27. Oliver G: Lymphatic vasculature development. Nat Rev Immunol 2004, 4:35–45
28. Hamed S, Ullmann Y, Egozi D, Daod E, Hellou E, Ashkar M, Gilhar A, Teot L: Fibronectin potentiates topical erythropoietin-induced wound repair in diabetic mice. J Invest Dermatol 2011, 131:1365–1374
29. Badr G: Supplementation with undenatured whey protein during diabetes mellitus improves the healing and closure of diabetic wounds through the rescue of functional long-lived wound macrophages. Cell Physiol Biochem 2012, 29:571–582
30. Ahmad J, Zubair M, Malik A, Siddiqui MA, Wangnoo SK: Cathepsin-D, Adiponectin, TNF-alpha, IL-6 and hsCRP plasma levels in subjects with diabetic foot and possible correlation with clinical variables: a multicentric study. Foot (Edinb) 2012, 22:194–199
31. Dave GS, Kalia K: Hyperglycemia induced oxidative stress in type-1 and type-2 diabetic patients with and without nephropathy. Cell Mol Biol (Noisy-le-grand) 2007, 53:68–78
32. Mahdavian Delavary B, van der Veer WM, van Egmond M, Niessen FB, Beelen RH: Macrophages in skin injury and repair. Immunobiology 2011, 216:753–762

# Visual Improvement after Cultivated Oral Mucosal Epithelial Transplantation

*Chie Sotozono, MD, PhD,[1] Tsutomu Inatomi, MD, PhD,[1] Takahiro Nakamura, MD, PhD,[1] Noriko Koizumi, MD, PhD,[1] Norihiko Yokoi, MD, PhD,[1] Mayumi Ueta, MD, PhD,[1] Kotone Matsuyama, BS,[2] Keiko Miyakoda, MS, MPH,[2] Hideaki Kaneda, MD, PhD,[2] Masanori Fukushima, MD, PhD,[2] Shigeru Kinoshita, MD, PhD[1]*

***Purpose:*** To report the effectiveness, disease-specific outcomes, and safety of cultivated oral mucosal epithelial sheet transplantation (COMET), with the primary objective of visual improvement.

***Design:*** Noncomparative, retrospective, interventional case series.

***Participants:*** This study involved 46 eyes in 40 patients with complete limbal stem cell deficiency (LSCD) who underwent COMET for visual improvement. These LSCD disorders fell into the following 4 categories: Stevens-Johnson syndrome (SJS; 21 eyes), ocular cicatricial pemphigoid (OCP; 10 eyes), thermal or chemical injury (7 eyes), or other diseases (8 eyes).

***Methods:*** Best-corrected visual acuity (BCVA) and ocular surface grading score were examined before surgery; at the 4th, 12th, and 24th postoperative week; and at the last follow-up. Data on COMET-related adverse events and postoperative management were collected. The outcomes in each disease category were evaluated separately.

***Main Outcome Measures:*** The primary outcome was the change in median logarithm of the minimum angle of resolution (logMAR) BCVA at the 24th postoperative week. The secondary outcome was the ocular surface grading score.

***Results:*** Median logMAR BCVA at baseline was 2.40 (range, 1.10 to 3.00). In SJS, logMAR BCVA improved significantly during the 24 weeks after surgery. In contrast, the BCVA in OCP was improved significantly only at the 4th postoperative week. In 6 of the 7 thermal or chemical injury cases, logMAR BCVA improved after planned penetrating keratoplasty or deep lamellar keratoplasty. Grading scores of ocular surface abnormalities improved in all categories. Of 31 patients with vision loss (logMAR BCVA, >2) at baseline, COMET produced improvement (logMAR BCVA, ≤2) in 15 patients (48%). Visual improvement was maintained with long-term follow-up (median, 28.7 months). Multivariate stepwise logistic regression analysis showed that corneal neovascularization and symblepharon were correlated significantly with logMAR BCVA improvement at the 24th postoperative week ($P = 0.0023$ and $P = 0.0173$, respectively). Although postoperative persistent epithelial defects and slight to moderate corneal infection occurred in the eyes of 16 and 2 patients, respectively, all were treated successfully with no eye perforation.

***Conclusions:*** Long-term visual improvement was achievable in cases of complete LSCD. Cultivated oral mucosal epithelial sheet transplantation offered substantial visual improvement even for patients with end-stage severe ocular surface disorders accompanying severe tear deficiency. Patients with corneal blindness such as SJS benefited from critical improvement of visual acuity.

***Financial Disclosure(s):*** The author(s) have no proprietary or commercial interest in anymaterials discussed in this article. *Ophthalmology 2013;120:193–200 © 2013 by the American Academy of Ophthalmology.*

Corneal renewal and repair are mediated by corneal epithelial stem cells situated mainly in the limbus, the narrow region between the cornea and the bulbar conjunctiva.[1] Damage or depletion of the corneal epithelial stem cells, known as limbal stem cell deficiency (LSCD), leads to conjunctival invasion that results in vascularization and scarring of the cornea with an associated profound loss of vision.[1] Limbal stem cell deficiency can be caused by Stevens-Johnson syndrome (SJS), ocular cicatricial pemphigoid (OCP), and thermal or chemical injury, which are all characterized by the loss of corneal epithelial stem cells. Such LSCD may cause severe ocular surface diseases (OSDs) in which cicatrization resulting from conjunctival fibrosis, symblepharon, and severe dry eye greatly disrupt visual function and can progress gradually with chronic inflammation.[2–4] To date, few effective medical or surgical treatments for severe OSDs have been available.[5–15]

Since 1998, the authors have used amniotic membrane transplantation to treat severe OSDs. Amniotic membrane exhibits an anti-inflammatory effect and also acts as a substrate for epithelialization.[16] The results of previous studies have shown that amniotic membrane transplantation alone[17,18] or amniotic membrane transplantation combined with limbal transplantation[6,19,20] promoted epithelialization, reduced pain, reconstructed the fornix, and minimized inflammation of the ocular surface to a remarkable degree in



ISSN 0161-6420/13/$–see front matter
http://dx.doi.org/10.1016/j.ophtha.2012.07.053

patients with severe OSDs. Based on these promising results, novel methods have been developed for the cultivation of allogeneic corneal[7,8,21] or autologous oral mucosal[22–25] epithelial cells on a denuded amniotic membrane. Immunologic rejection and increased risk of infection or systemic adverse effects associated with the long-term immunosuppressive therapy accompanying allograft transplantation[6] encouraged changing to autologous cultivated oral mucosal epithelial transplantation (COMET) in patients with severe OSDs in 2002.[10,11,23,26]

To clarify the effectiveness, disease-specific outcomes, and safety of COMET, all of the clinical data from all 72 patients that the authors treated with COMET since 2002 were analyzed. The objective of this present study was to summarize the long-term clinical outcomes of 40 of those 72 patients who underwent COMET with the primary objective of visual improvement between June 2002 and December 2008.

## Patients and Methods

### Patients

Autologous COMET was performed on consecutive patients who were diagnosed with total LSCD based on the complete disappearance of the palisades of Vogt and 360° of conjunctivalization.[1] The COMET treatment protocol was approved by the ethical review board of Kyoto Prefectural University of Medicine, Kyoto, Japan, in 2002. The final decision to perform COMET was made by the university's team of corneal specialists. Before the surgery, written informed consent was obtained from all patients in accordance with the tenets of the Declaration of Helsinki for research involving human subjects. The current retrospective study used an itemized data collection form, and the medical records of all patients who underwent COMET between June 2002 and December 2008 were examined retrospectively. This retrospective study protocol was approved by the ethical review board of Kyoto Prefectural University of Medicine in 2009. In this study, 40 of the 72 patients who underwent COMET were analyzed with the primary objective of visual improvement.

### Cell Culture

All of the COMET sheets were prepared at the good manufacturing practices–graded Cell Processing Center at Kyoto Prefectural University of Medicine as previously described.[23,26] Autologous oral mucosal epithelial cells were obtained from a 6-mm–diameter biopsy specimen obtained from each patient's buccal mucosa, and the cells then were cultured on an amniotic membrane spread on the bottom of a culture insert and were cocultured with mitomycin C-inactivated 3T3 fibroblasts (NIH-3T34; RIKEN Cell Bank, Tsukuba, Japan). The cultured cells were submerged in medium for approximately 1 week and then were exposed to air by lowering the medium level (airlifting) for 1 to 2 days. All amniotic membrane was obtained from caesarean sections according to the preparation method described previously.[23] Although fetal bovine serum initially was used as a culture medium, autologous serum was used in later cultures to reduce the risk of transmitting nonhuman pathogens.[26]

### Transplantation and Postoperative Management

The surgical procedure (see the Supplemental Video, available at http://aaojournal.org) and postoperative management have been described previously.[24,25] In patients with severe symblepharon or a large area of bare sclera exposed during surgery, amniotic membrane was transplanted onto the bare sclera to reconstruct conjunctival fornices.[18] In patients with a cataract, phacoemulsification and aspiration plus intraocular lens implantation were performed simultaneously with COMET. No penetrating keratoplasty or deep lamellar keratoplasty was performed simultaneously with COMET. For patients with severe corneal stromal opacity, a 2-step surgical approach was planned, with the first step being COMET and the second step being either penetrating or deep lamellar keratoplasty.[25]

Systemic corticosteroid (betamethasone, 1 mg/day) and cyclosporine (2 to 3 mg/kg daily) were administered to prevent postoperative inflammation and immunologic response and then were tapered, depending on the clinical findings. Dexamethasone (0.1%) and antibiotic eye drops were instilled 4 times daily. Dry-eye patients were administered artificial tears. A therapeutic soft contact lens was used for at least 1 month to protect transplanted epithelium from mechanical ablation.

### Postoperative Follow-up and Outcomes

Best-corrected visual acuity (BCVA) was converted to the logarithm of the minimum angle of resolution (logMAR). Ocular surface conditions including corneal appearance (epithelial defects, clinical conjunctivalization, neovascularization, opacification, keratinization, and symblepharon) were graded by at least 2 ophthalmologists (C.S., T.I., and T.N.) on a scale from 0 to 3 according to their severity, in accordance with a previously reported grading system.[27] Severe OSDs are characterized by an associated loss of conjunctival stem cells, and the severity of conjunctival involvement affects the visual prognosis. Therefore, findings on upper and lower fornix shortening were added to evaluate the grade of conjunctival appearance. Fornix shortening was graded from 0 to 3 based on the following clinical features: normal depth (grade 0), shortened by less than one quarter (grade 1), shortened by one quarter to one half (grade 2), and shortened by more than one half (grade 3). Upper and lower fornix shortenings were graded separately. The sum of each grading score was defined as the ocular surface grading score (maximum, 24).

Each patients logMAR BCVA, ocular surface grading score, and data on adverse events related to COMET or postoperative management were collected from the medical records at these specific time points: before surgery; at the 4th, 12th, and 24th postoperative weeks; and at the last follow-up examination. The primary outcome was the change in logMAR BCVA at the 24th postoperative week. Because other ocular diseases can affect this visual outcome, a secondary outcome, the ocular surface grading score, also was defined.

### Statistical Analysis

The change in BCVA and ocular surface grading score from baseline at each visit, except for the last visit, was analyzed using the Wilcoxon signed-rank test in each disease category (SJS, OCP, thermal or chemical injury) except for other diseases. Multivariate stepwise logistic regression analysis was used to determine the factors influencing visual improvement.

This study defined the critical visual improvement rate as the proportion of patients in whom BCVA at the 24th postoperative week had improved to at least 0.01, as a percentage of the patients with a BCVA of less than 0.01 at baseline. Patients with a visual acuity of 0.01 or more can read and walk using vision aids. Thus, an improvement to at least 0.01 indicates a capacity for independence in daily life. If data were missing from the 24th postoperative week, data from follow-up at the last visit were substituted.